International
Progress Report

IPR-05-39

Äspö Hard Rock Laboratory

TRUE Block Scale continuation project

Evaluation of the BS2B sorbing tracer tests using the LASAR approach

Hua Cheng
Vladimir Cvetkovic

Water Resources Engineering,
Royal Institute of Technology, KTH

Luly 2005

Svensk Kärnbränslehantering AB
Swedish Nuclear Fuel
and Waste Management Co
Box 5864
SE-102 40 Stockholm Sweden
Tel 08-459 84 00
+46 8 459 84 00
Fax 08-661 57 19
+46 8 661 57 19

Äspö Hard Rock
Laboratory

Report no.
IPR-05-39
No.
F56K
Author
Hua Cheng
Vladimir Cvetkovic
Date
July 2005
Checked by
Anders Winberg
Date
September 2006
Approved
Anders Sjöland
Date
2006-11-29

Äspö Hard Rock Laboratory

TRUE Block Scale continuation project

Evaluation of the BS2B sorbing tracer tests using the LASAR approach

Hua Cheng
Vladimir Cvetkovic

Water Resources Engineering,
Royal Institute of Technology, KTH

July 2005

Keywords: Fault, Fracture, heterogeneity, In-situ, Prediction, Retention, Sorbing, Tracer

Abstract

This report presents modelling results for the SKB KTH-WRE prediction and evaluation modelling of the BS2B sorbing tracer test as part of the TRUE Block Scale Continuation project.

Two flow paths were selected for the BS2b tests. Flow path I is situated in a single Type 1 (fault) structure (Structure #19) with a length of approximately 20 m. Flow path II starts in background fracture BG1 and ends in Structure #19.

The prediction of the breakthrough curves (BTCs) in the BS2b tests has been conducted by calibrating the results of the conservative pre-tests CPT-4b and CPT-4c performed in the same flow paths. The prediction results generally matched the measured BTCs well for Flow path I, although overestimating the retention of Rb-86. For Flow path II, the retention of all tracers was underestimated.

The evaluation was performed by assuming effective (uniform) retention parameters and by accounting for depth-wise heterogeneity of retention parameters normal to the fracture surface. The evaluation results indicated that the underestimation or overestimation of retention probably is due to an underestimation or overestimation of the sorption processes in rock matrix, as represented by K_d.

In the penetration analysis for individual flow paths, Flow path I is assumed to consist primarily of Type 1 structure (fault). Flow path II is assumed to consist only of Type 2 structure as the background fracture BG1 (possibly in combination with additional background fractures) which probably dominantly determine the retention in this path. Comparison of the estimated parameters of the material retention property group κ from two different methods indicates that they differ by a factor of 0.4 to1.4 for all tracers except for Rb-86, for which the factor is 3.

The parameter κ of BG1 was inferred indirectly, by using κ of Structure #19 calibrated from the BTCs of flow path I. We find that the parameter κ of BG1 is lower by a factor of 2 –9 compared to that of Structure #19, but the hydrodynamic control parameter β is one order of magnitude higher due to higher water residence time and smaller aperture. These estimates are uncertain, in particular for the hydrodynamic control parameter, nevertheless the results provide a clear indication that although the retention properties are weaker in BG1, the overall retention is stronger in BG1 than in Structure #19.

Sammanfattning

Denna rapport presenterar modelleringsresultat för SKB KTH-WREs prediktion och utvärderingsmodellering av försök med sorberande spårämnen (BS2B) inom projektet TRUE Block Scale Continuation.

Två flödesvägar har studerats i BS2B-försöket. Flödesväg I är belägen i en ensam Typ 1(fault)-struktur (Struktur 19) med en längd av ungefär 20 m. Flödesväg II börjar i bakgrundssprickan BG1 och slutar i Struktur 19.

Prediktionen av genombrottskurvorna (BTC) i BS2B-försöket gjordes genom att vi kalibrerade resultaten av de icke-reativa förförsöken CPT-4b och CPT-4c, genomförda i samma flödesvägar. Prediktionerna stämde i allmänhet väl överens med BTCs för flödesväg I, men överskattade retentionen hos Rb-86. För flödesväg II underskattades retentionen hos samtliga spårämnen.

Utvärderingen genomfördes genom att anta effektiva (konstanta) retentionsparametrar och genom att ta hänsyn till heterogeniteten hos retentionsparametrarna vinkelrät mot sprickytan. Utvärderingsresultaten indikerar att över- och underskattningarna av retentionen troligt uppkommer på grund av över- och underskattningar av sorptionsprocesserna i bergmatrisen, här representerade av K_d.

I penetrationsanalysen för enskilda flödesvägar, antas flödesväg I bestå huvudsakligen av Typ 1-struktur (fault). Flödesväg II antas bestå enbart av Typ 2-struktur/-er, då bakgrundssprickan BG1 (möjligtvis i kombination med ytterligare bakgrundssprickor) troligtvis är den förhärskande faktorn som avgör retentionen i denna flödesväg.. En jämförelse av uppskattade parametrar för retentionsegenskapsgruppen κ från två olika metoder visar att de skiljer sig med en faktor 0.4 till 1.4 för alla spårämnen utom för Rb-86, där faktorn är 3.

Vi bestämde parametern materialegenskapsgruppen κ hos BG1 indirekt, genom att använda κ hos Struktur 19, kalibrerad av BTCs i den första flödesvägen. Vi finner att parametern κ hos BG1 är en faktor 2-9 lägre än den hos Struktur 19, medan den hydrodynamiskt kontrollerade parametern β är en storleksordning högre på grund av längre vattenuppehållstider och mindre spricköppning. Dessa uppskattningar är osäkra, speciellt för den hydrodynamiska kontrollparametern, men resultaten ger en klar indikation att trots att rententionsegenskaperna är svagare i BG1, är den totala retentionen högre i flödesvägen med bakgrundssprickor (inklusive BG1) än i Struktur 19.

Contents

List of Figures

List of Tables

1 Introduction

1.1 Background

To improve the understanding of radionuclide retention mechanisms in the Swedish crystalline rock, Swedish Nuclear Fuel and Waste Management Company (SKB) has initiated a tracer test program referred to as Tracer Retention Understanding Experiments (TRUE) (Bäckblom and Olsson, 1994). The basic idea of the TRUE program is to perform a series of experiments with increasing complexity in terms of the involved retention processes and spatial scale, and to verify the capability of various modelling approaches in predicting radionuclide migration and retention. The TRUE experiments were performed at the Äspö Hard Rock Laboratory (HRL) in southeastern Sweden, and have progressed in different stages. The first stage (TRUE-1) was focused on a detailed scale (<10 m) in a single feature (e.g., Cvetkovic et al., 2000; Winberg et al., 2000). The basic objective of TRUE-1 was to perform and analyze transport experiments with non-sorbing and sorbing tracers in a discrete singular fracture in crystalline rock. The second stage was performed on a block scale (10 – 50 m) with possible multiple geological structures (e.g., Cvetkovic and Cheng, 2002; Poteri et al., 2002). The Block Scale tracer tests aimed at providing data and facilitating modelling of tracer transport in a fracture network in a block scale. The location of the detailed scale test (TRUE-1) at the Äspö HRL is in the northeastern part of the underground laboratory, while the block scale test site is located in the southwestern part of the experimental level at the Äspö HRL.

When the TRUE Block Scale project was finished, it was recognized that some issues were still unclear. To further address these issues, the TRUE Block Scale Continuation project was launched in 2001. The overall objective has been to increase the understanding of the transport and retention of sorbing species over long distances (10-100 m) possibly in a fracture network involving background fracture in a new location at the TRUE Block Scale site. The TRUE Block Scale Continuation project has been conducted in two stages: the BS2A and the BS2B

1.2 Objectives

The aim of the BS2A was to perform complementary investigations to support the BS2B studies, among other things to analyse plausible test scales and the likelihood of assessing effects of microstructure heterogeneity (e.g., Cvetkovic, 2003). The BS2B studies aimed at performing radioactive sorbing tracer tests involving background fractures preceded by model prediction and subsequently by evaluation modelling. In the BS2B studies the sorbing tracer tests were performed in TRUE Block Scale site in the area surrounding Structure #19. Two flow paths were selected for the BS2B tests (Andersson et al., 2004, 2005). Flow path I was in a single Type 1 (fault) structure (c.f. Dershowitz et al., 2003) over length scales of tens of meters. The 19.5 m long flow path KI0025F02:R3 → KI0025F03:R3 in Structure #19 was chosen. Flow path II contained a single background fracture of Type 2 (non-fault, c.f Dershowitz et al., 2003) connected to a major Type 1 structure, possibly by way of a network of background fractures of yet unknown geometry. The only flow path available for a tracer experiment addressing this type of transport was the long flow path KI0025F02:R2 (BG1) → KI0025F03:R3 (Structure #19), with an Euclidian length of aabout 22 m, but most likely about twice this length in reality .

The specific objectives of the BS2B studies are to test the validity of the following hypotheses:

- **Hypothesis I a)** Microstructural (i.e., detailed geological, mineralogical and
- geochemical) information can provide significant support for predicting transport of sorbing solutes at experimental time scales,
- **Hypothesis I b)** Transport at experimental time scales is significantly different for faults (significant alteration, brecciation and fault gouge) and joints (with or without alteration), due to the indicated differences in microstructure and properties,
- ***Hypothesis I c)*** Longer distance pathways are dominated by fault rock zone behaviour, while shorter pathways (say representative for fractures in the vicinity of a deposition hole) may be more likely to be dominated by joint fracture characteristics.
- ***Hypothesis II c)*** Fracture retention properties tend to be scale-dependent primarily due to differences in microstructure.

Hypothesis Ia) concerns the use of microstructural information for prediction of tracer transport. Our predictions have been based on calibration of pre-tests for conservative tracers performed in the same flow path. The defined two structure types (Dershowitz et al., 2003; Tullborg and Hermanson, 2004) have not been used explicitly in our predictions. However the K_d and K_a values provided by Byegård and Tullborg, (2004) have been used in this context to arrive at effective retention parameters for the complete sequence of stratified immobile retention zones of the respective structure types and/or flow paths (see next section).

Hypothesis Ib) regards the difference of transport between faults and joints. The BS2B tests were performed in two flow paths involving both types of structures (faults and joints). Evaluation of BS2B addresses Hypothesis Ib).

In summary, the KTH/WRE modelling work has focused on prediction and evaluation of the measured BTCs for the BS2B tests. The evaluation work is related primarily to Hypothesis Ib), and also to Hypothesis Ia).

1.3 Results of laboratory program

Laboratory experiments were performed to study sorption and diffusion of tracers on two major types of materials for Structure #19 and the background fracture BG1: fault gouge materials and rim zone materials. Both types of the materials are obtained from the TRUE Block Scale site. The detailed results of the laboratory programme are reported by /Byegård and Tullborg, 2004/; /Byegård, in prep/.

For Structure #19, the fault gouge materials were sampled from KI0025F02 intercept of Structure #19. While for background fracture BG1, the gouge materials were sampled from borehole KI0023B of Structure #20. The rim zone materials were sampled from the intercept in KI0023B (strongly hydrothermally altered rock, 80%) and the intercept in KI0025F (mylonitic and cataclasitic wall rock in Äspö diorite, 20%) for Structure #19. For the rim zone of BG1, estimation of the K_a and K_d parameter is based on the altered Äspö diorite in Feature A intercept with borehole KXTT2 in the TRUE-1 project (Winberg et al., 2000).

For the purpose of prediction of the BS2B tests, /Byegårds and Tullborg, 2004/ proposed K_a and K_d values for the sorbing tracers based on the laboratory experiments from the sampled gouge materials and the rim zone materials. The proposed K_a and K_d parameters are summarized in Table 1-1. Note that the rim zone materials include two types of rock material: Cataclasite/mylonitic rock and altered rock.

Table 1-1 Summary of K_d values for the gouge material and the rim zone material /Byegård and Tullborg, 2004/.

Tracer	Structure	Gouge	Rim zone Cataclasite		Rim zone Altered rock	
		K_d (m^3/kg)	K_d (m^3/kg)	K_a (m)	K_d (m^3/kg)	K_a (m)
$^{85}Sr^{2+}$	#19	6.0e-4	1.4e-4	2.2E-5	2.6e-5	1.5E-5
$^{86}Rb^{+}$	#19	2.7e-3	4e-3	<8E-4	4e-4	<1E-4
$^{137}Cs^{+}$	#19	4.0e-2	3e-2	9.8E-3	5e-4	1.0E-3
$^{22}Na^{+}$	BG1	2.0e-4	-	-	1.7e-6	7.0E-7
$^{133}Ba^{2+}$	BG1	2.7e-2	-	-	6.9e-4	2.9E-4
$^{54}Mn^{2+}$	BG1	1.7e-1	-	-	4.3e-3	1.8E-3*

The upper-limit values are taken if the data are given in a range instead of a single value /Byegård and Tullborg, 2004/.

1.4 Outline of report

In Chapter 2 we present the LaSAR approach that is used for evaluating the BTC data of the BS2B sorbing tracer tests from the TRUE Block Scale Continuation project. In Chapter 3 we summarize the BS2B tracer tests and the preceding conservative tracer pre-tests performed in the same flow paths used for the BS2B tests. In Chapter 4 we present prediction results and compare them with the experimental data. In Chapter 5 we present evaluation results using effective retention parameters from calibration. In Chapter 6 we investigate the effects of retention heterogeneity to provide estimates for depth-dependent retention parameters, and compare them with the parameters obtained from the evaluation based on the calibration procedure in Chapter 5. In Chapter 7 we discuss the results. In Chapter 8 we summarize our results and conclusions.

2 Evaluation model

2.1 LASAR approach

The Lagrangian Stochastic Advective Reaction (LaSAR) framework is used in this work as a prediction and evaluation model. A more detailed account of the model is presented in Cvetkovic et al. (1999). The same framework has been applied for prediction and evaluation modelling in the first stage of the TRUE tracer test program (TRUE-1) (Cvetkovic et al., 2000). The framework was extended from a single heterogeneous fracture to a network of heterogeneous fractures and applied for modelling the TRUE Block Scale tracer tests (Cvetkovic and Cheng, 2002). The LaSAR approach is also employed in the Task 6 modelling within the framework of the Äspö Task Force on modelling of groundwater flow and solute transport (Cheng and Cvetkovic, 2004).

2.2 Transport model

The governing equations for the transport of tracers can be written as

$$\frac{\partial q}{\partial t}+\frac{\partial q}{\partial \tau}=\frac{D\theta}{b(\tau)}\frac{\partial N^{*}}{\partial z}-\frac{K_a}{b(\tau)}\frac{\partial q}{\partial t} \tag{2-1}$$

$$\frac{\partial N^{*}}{\partial t}-D\frac{\partial^2 N^{*}}{\partial z^2}=-K_d^m\frac{\partial N^{*}}{\partial t} \tag{2-2}$$

where t [T] is time; τ [T] is advective travel time; q [M L^{-2} T^{-1}] = $C\,V$ is the tracer breakthrough in the fracture and N^{*} [M L^{-2} T^{-1}]= $N\,V$; C [ML^{-3}] is mobile concentration; N [ML^{-3}] is immobile concentration; V[LT^{-1}] is advective velocity.

Solution for a single flow path

The solution of Equations (2-1) and (2-2) can be obtained for a single trajectory using the Laplace transform (e.g., Selroors and Cvetkovic, 1996):

$$q(x,t;\tau)=\rho_0\gamma(t,\tau;\beta) \tag{2-3}$$

where ρ_0 is the initial solute mass. The function γ is defined as

$$\gamma(t,\tau;\beta)=\frac{H(t-\tau)B}{2\sqrt{\pi}(t-\tau-A)^{3/2}}\exp\left[-\frac{B^2}{(t-\tau-\beta A)}\right] \tag{2-4}$$

where

$$B = \sum_{j=1}^{M} \beta_j \kappa_j \; ; \qquad \beta_j = \frac{l_j}{V_j b_j}; \qquad \tau_j = \frac{l_j}{V_j} \tag{2-5}$$

$$A = \sum_{j=1}^{M} K_a^j \beta_j \; ; \qquad \kappa_j \equiv \theta_j \left[D_j (1 + \frac{\rho_b K_d^j}{\theta_j}) \right]^{1/2} \tag{2-6}$$

and γ[1/T] is the probability density function of the residence time for a single tracer particle travelling from the injection section to the pumping section, under the influence of the processes of advection, diffusion and sorption. γ is conditioned on the parameter *A* and *B*; and *H* is the Heaviside step function. The index "*j*" designates either the *j*th fracture (if the particle is transported through a series of fractures), and/or the *j*th discretization segment of a single heterogeneous fracture; *M* is the total number of segments, which could also extend through a series of heterogeneous fractures; K_d [L^3 M^{-1}] is the sorption distribution coefficient of the rock matrix; K_a [L] is the sorption coefficient on the fracture surface; *b* is the fracture half-aperture; *D* [L^2 T^{-1}] is the pore diffusivity and ρ_b is the density of the rock matrix. θ[-] is porosity. All of the above parameters are generally segment-dependent. They are all therefore assigned the index "*j*".

Note that Equations (2-4) to (2-6) are applicable to a single trajectory (e.g., the *i*th trajectory). We may have a number of trajectories (e.g., *N* trajectories in this simulation).

In Equation (2-4) two parameter groups *B* and *A* control γ/Cvetkovic and Cheng, 2002/. The quantity *B* is further informed by β and κ. Here β is purely a flow dependent quantity that accounts for hydrodynamic control of retention.. Since κ is a parameter describing the diffusion and sorption in the rock matrix (Eq. 2-7), the effect of aperture variation on matrix diffusion/sorption is accounted for by the product $\beta\kappa$. On the other hand, the effect of aperture variation on surface sorption is described by the parameter *A* determined by the product βK_a in Equation (2-4). If the retention parameters θ, K_d, D are constant (effective) values for all segments, we have

$$B = \beta k; \quad \kappa = \theta \sqrt{\mathrm{D}(1 + \frac{\mathrm{K_d}\rho}{\theta})}; \quad \beta = \sum_{\mathrm{i=1}}^{\mathrm{N}} \frac{l_i}{V_i b_i}; \quad A = kK_a \tag{2-7}$$

Our basic evaluation model is based on (Eq. 2-7).

Dispersive effects

Dispersion in a fracture network arises when there is a random variation of the advection velocity. The solute particles in the fluid are advected along different streamlines with random variation of the fluid velocity, thus τ and β are random variables. The solution γ in Equation (2-4) is applicable to a single trajectory that will depend on (or is conditioned on) the random values of τ and β.

Let $g(\tau, \beta)$ denote the joint probability density function (PDF) of τ and β at a pumping or controlling section. This PDF can in principle be computed using particle tracking (Monte Carlo simulations) (e.g., Cvetkovic et al., 1999). If $g(\tau, \beta)$ is known, and γ is available in a closed form, the solute discharge, Q, (or the breakthrough curve, BTC), at the pumping section can be evaluated as:

$$Q(t) = \int_0^\infty \phi(t - t')dt' \int_0^\infty \gamma(t', \tau; \beta) g(\tau, \beta) d\tau d\beta \qquad (2\text{-}8)$$

where $\phi(t)$ is the injection function. There is, however, a strong correlation between τ and β as indicated by numerical simulations (e.g., Cvetkovic et al., 1999). It is, therefore, possible to approximate the correlation by a deterministic relation between τ and β, and to attribute all the dispersive effects due to velocity variations to the residence time PDF for pure advection, $g(\tau)$. The numerical simulation under various conditions have indicated that β and τ are strongly correlated, and related by a power law $\beta \sim \tau^m$ (Cvetkovic et al., 1999, Cheng et al., 2003, Cheng and Cvetkovic, 2005). However, for the experimental conditions encountered in TRUE site, a linear relationship seems to provide a reasonable approximation (Cvetkovic et al., 2000, Cvetkovic and Cheng, 2002). We therefore assume

$$\beta = k\tau \qquad (2\text{-}9)$$

where k is an in-situ parameter associated with a given flow path. Equation (2-9) simplifies the evaluation problem significantly, since the entire distribution of β is replaced by the distribution of τ and a parameter k. The k has been referred to as the flow-wetted surface per unit volume of water (Andersson et al., 1998).

Substituting (2-9) into (2-7) and (2-4), we get $A=\tau\zeta$ and $B=\tau\psi$ where the ζ and ψ are the two key parameter groups defined by

$$\varsigma \equiv kK_a; \ \psi = k\kappa \qquad (2\text{-}10)$$

The remaining problem is then to determine $g(\tau)$. If $g(\tau)$ is known, the solute discharge Q is evaluated as:

$$Q(t) = \int_0^t \phi(t - t')dt' \int_0^\infty \gamma[t', \tau; \beta(\tau)] g(\tau) d\tau \qquad (2\text{-}11)$$

where $\beta(\tau)$ is given in (2-9), and γ is given by (Eq. 2-4).

2.3 Calibration

Evaluation of the measured BTCs is conducted in two calibration steps:

- Determination of $g(\tau)$ by deconvoluting the BTCs of conservative tracers. The actual form of $g(\tau)$ is usually assumed to be an inverse-Gaussian distribution. The first two moments of the water residence time distribution are calibrated for each flow path.
- Calibration of the two parameter groups ζ and ψ on the measured BTC data for each flow path using the deconvoluted $g(\tau)$ from the first step.

2.4 Accounting for heterogeneity

Equations (2.4)-(2.6) directly account for the horizontal heterogeneity in the lateral x,y directions of the fracture plane. Retention parameters in Equations (2.5)-(2.6) are assumed to be constant in the direction normal to the fracture plane (z-direction) into the fracture wall rock. For a schematic presentation of the immobile retention zones, see Cvetkovic and Cheng, (2002).

It is clear that the retention parameters are spatially variable along the fracture plane. There is also evidence that the porosity decreases with increasing *z* in and near the fracture surfaces and so does possible also the K_d . For instance in the Task 6C microstructural model (referred to as Task 6C model hereafter), both θ and K_d are assumed to decrease with increasing *z* (Dershowitz et al., 2003). The key issue related to heterogeneity in the *z*-direction is the penetration depth for individual tracers, the latter of variable diffusivity and sorbtivity.

The retention parameters of Equation (2-7) are effective values for the effective immobile zone for individual tracers. We will estimate effective in-situ values of ζ and ψ for all tracers and flow paths by calibrating relevant pretests on BS2B data in preparation for the predictions (Chapter 4) and subsequent evaluation (Chapter 5).

In the Task 6C model, two fracture types including properties (θ and K_d, etc) of various retention zones were defined. In Chapter 6 we make an attempt to account for heterogeneity in the *z*-direction by estimating the penetration depth for different tracers, and using the evaluated penetration depths to define a depth-averaged, tracer-dependent effective porosity θ (and K_d), based on the microstructural model and parameterisation.

3 Summary of tracer test results

3.1 Experimental site

The BS2B tests have been performed at the TRUE Block Scale test site in two different flow paths. The first path (Path I) is assumed contained within a single Type 1 structure (#19) between borehole sections KI0025F02:R3 and KI0025F03:R3. The second flow path (Path II) includes a single background Type 2 fracture connected to a major Type 1 structure (#19), possibly by way of a network of additional background fractures. The available flow path for the purpose is the path between boreholes KI0025F02R2 (BG#1) and KI0025F03R3 (#19).

Locations of the boreholes and involved borehole sections in the TRUE Block Scale array are shown in Figure 3-1 together with the main interpreted deterministic structures in the investigated rock volume, including Structure #19.

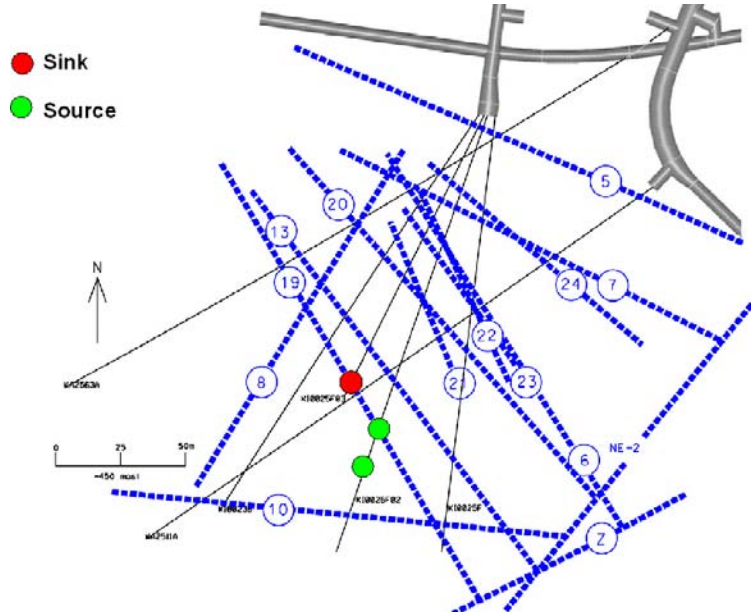

Figure 3-1. *Location of injection sections (green symbols) and pumping section (red symbol) in the TRUE Block Scale experimental site (from Andersson et al., 2005).*

3.2 Conservative tracer tests

The characteristics of the CPT-4b and CPT-4c tests (Andersson et al., 2004), which were performed as preparatory tests for the subsequent BS2B sorbing tracer tests are summarized in Table 3-1, Figure 3-2 and Figure 3-3. The CPT-4a test is a radially converging test performed in Path I. The CPT-4b test is a weak dipole test performed in Path II. The tests were performed in a radially converging flow field with a withdrawal rate of Q=2.8 l/min at the start that decreases slowly to Q=2.6 l/min at the termination of the test.

Table 3-1. Summary of conservative tracer pre-tests performed on the same flow paths as used in the BS2B tests.

Test	Inj. Rate (ml/h)	Inj. Borehole (#structure)	Pump borehole	Tracer	Recovery (%)
CPT-4c (Path I)	262	KI0025F02:R3 (#19)	KI0025F03:R3 (#19)	Uranine	84
CPT-4b (Path II)	72	KI0025F02:R2 (#25)	KI0025F03:R3 (#19)	Amino.G	79

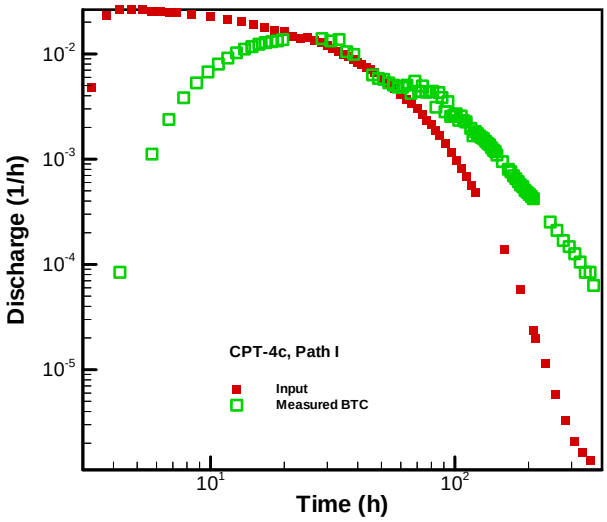

Figure 3-2. *Measured injection function (red) and measured BTC data (green) of the CPT-4c test for Uranine in Path I.*

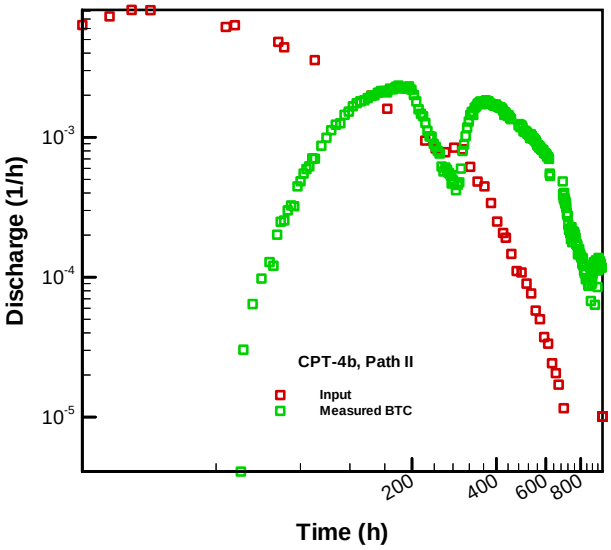

Figure 3-3. *Measured injection function (red) and measured BTC data (green) of the CPT-4b test for Amino G. in Path II.*

3.3 BS2B sorbing tracer tests

The BS2B sorbing tracer test was performed with injection of tracer in both flow paths I and II. The characteristics of the BS2B tests are summarized in Table 3-2. The normalized BTC data measured in the BS2B tests are plotted in Figures 3-4 and 3-5.

Table 3-2. Summary of the BS2B tests.

Path	Inj. Borehole (#structure)	Inj. Rate (ml/h)	Pumping borehole (#structure)	Pumping rate (l/min)	Tracers	Recovery (%)
I	KI0025F02:R3 (#19)	252	KI0025F03:R3 (#19)	2.3 – 2.5	$^{131}I^-$	80
					^{160}Tb-DTPA	87
					$^{85}Sr^{2+}$	86
					$^{86}Rb^+$	56
					$^{137}Cs^+$	28
II	KI0025F02:R2 (BG1)	69	KI0025F03:R3 (#19)	2.3 – 2.5	HTO	68
					^{155}Eu-DTPA	92
					$^{22}Na^+$	72
					$^{133}Ba^{2+}$	8
					$^{54}Mn^{2+}$	1

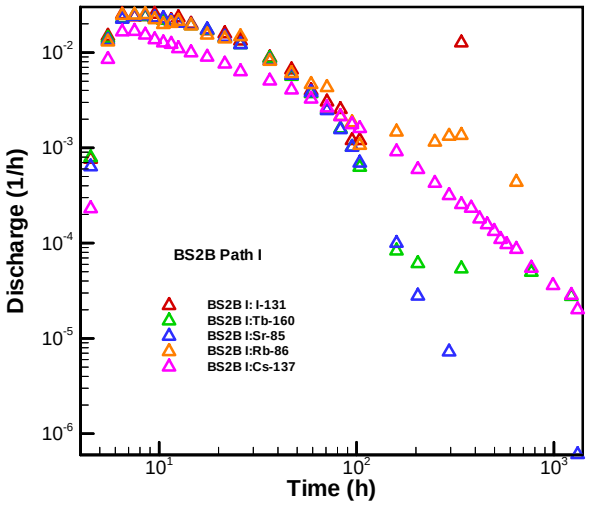

Figure 3-4. *Summary of the BTC data (normalized) measured in the BS2B tests for Path I.*

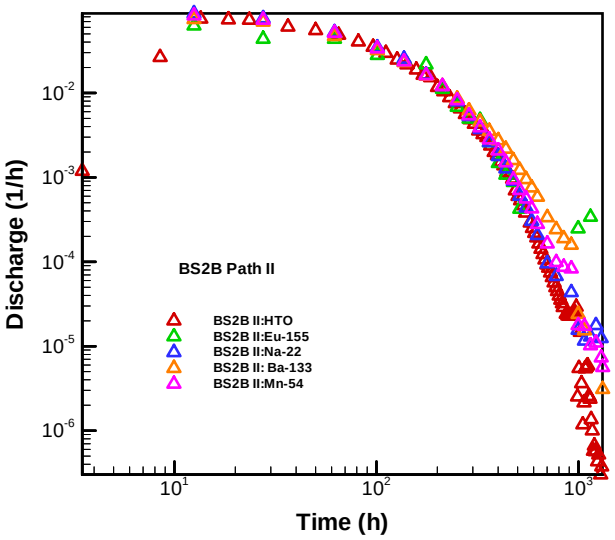

Figure 3-5. *Summary of the BTC data (normalized) measured in the BS2B tests for Path II.*

4 Prediction

The model predictions of the BS2B sorbing tracer test was conducted by calibrating on the relevant non-sorbing tracer tests CPT-4c (Path I) and CPT-4b (Path II), followed by forward prediction of the BS2B tests.

4.1 Prediction procedure

The prediction is performed using the retention parameters (K_a and K_d) obtained for the rim zone material (Table 1-1). The fracture rim zone material of Structure #19 consists of approximately 80% of "strongly hydrothermally altered rock" represented by the intercept in KI0023B and 20% of "mylonitic and cataclasitic wall rock, in Äspö diorite" represented by the intercept in borehole KI0025F.

For the purpose of the prediction and evaluation of the BS2B tests, the microstructural model is proposed by /Tullborg and Hermanson,2004/ based on the Task 6C model (Dershowitz et al., 2003). Structure #19 is considered to be a deterministic structure of Type 1 in the microstructural model. The fracture coating in the model is considered to be equivalent to the fracture surface where the sorption is assumed to be representative by K_a of the fracture rim zone material. The retention zones of cataclasite and the altered rock in the Type 1 structure of the microstructural model are consistent with the composition of the rim zone material from /Byegård and Tullborg, 2004/. Background fracture BG1 is considered as a Type 2 rock. The rim zone material of BG1 is the altered Äspö diorite which is also consistent with the definition of the Type 2 structure.

In the following, the prediction procedure is summarized both for flow paths I and II:

Path I: KI0025F02:R3(#19) $\rightarrow$ KI0025F03:R3 (#19)

- Determine $g(\tau)$, ψ by deconvoluting BTC of Uranine from the CPT-4c test. The actual form of $g(\tau)$ was assumed to be inverse-Gaussian (Cvetkovic and Cheng, 2002), and three parameters were calibrated; the first two moments of τ and the parameter ψ.Estimate k and κ based on the obtained ψ vales from the first step,
- Estimate the porosity θ, by assuming Archie's law

$$F = 0.71\theta^{1.58} \qquad (4\text{-}1)$$

from the obtained κ. For the nonsorbing tracer, $\kappa = \sqrt{\theta F D_w}$ where D_w is the diffusivity in water.

- Assume that the estimated θ value is applicable for all tracers involved in the BS2B tests in Path I,
- Determine effective values of K_d and K_a for each sorbing tracer, the effective K_d and K_a values are obtained from the values for the fracture rim zone (Table 1-1).
- The actual procedure of determining K_d and K_a values is presented later in this report.

Path II: KI0025F02:R2(BG1) → KI0025F03:R3 (#19)

- Determine $g(\tau)$, ψ by deconvoluting BTC of Amino G from the CPT-4b test.
- The remaining steps are the same as those mentioned for Path I above

For more information on calibration procedure, see Cvetkovic et al., (2000) and Cvetkovic and Cheng, (2002).

4.2 Calibration results

The temporal moments and the parameter ψ, calibrated from the CPT-4c pre-test for Path I and from the CPT-4b pre-test for Path II, are presented in Table 4-1. The calibrated BTCs are compared with the measured data in Figure 4-1 for Path I and in Figure 4-2 for Path II, respectively.

Table 4-1. Summary of calibrated temporal moments and parameter ψ

Path	$<\tau>$ (hour)	σ_τ^2 (hour^2)	ψ (h$^{-1/2}$)
I	14	160	0.13
II	200	15000	0.017

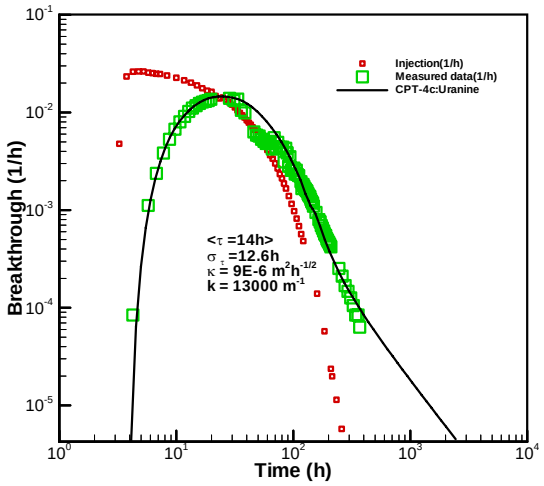

Figure 4-1. *Calibration on the BTC of Uranine in CPT-4c test.*

We have obtained the calibrated parameter group ψ for every flow path. There could be various combinations of k and κ values for the calibrated ψ value. Table 4-2 presents some possible combinations of k and κ values for Path I. All the combinations given in Table 4-2 are in principle equally possible, and give the same match between the modelled and experimental BTC shown in Figure 4-1. However, only one of them can be selected for the prediction of sorbing tracer BTCs. Note that although all the parameter combinations given in Table 4-2 provide the same match of the measured BTCs for Uranine in CPT-4c test, different parameter combinations would provide different modelling BTCs for sorbing tracers in terms of different *k* and θ values.

However, following the definition of β (Eq. 2-9), k can be interpreted as an inverse effective half-aperture. If we refer to Task 6C model, Structure #19 was assigned an effective aperture of 0.147 mm (Dershowitz, et al., 2003) which corresponds to an effective k value of 13000 m^{-1}. The estimated κ value is thus obtained as κ=1e-5 $mh^{-1/2}$ (green colour in Table 4-2). By using Archie's law (Eq. 4-1), a corresponding porosity of θ = 2.56% was obtained for κ=1e-5 $m/h^{1/2}$.

Table 4-2 Estimation table of k and κ values for ψ = 0.13($h^{-1/2}$), and the corresponding aperture and porosity value for Path I.

k (m^{-1})	Aperture(mm)	κ ($m/h^{1/2}$)	θ(%)
5000	0.4	4.33e-5	8.0
9000	0.22	1.44e-5	3.40
13000	0.15	1e-5	2.56
17000	0.12	7.65e-6	2.02
21000	0.095	6.19e-6	1.77

In summary, the following parameters were obtained by calibrating on the BTC of Uranine in the CPT-4c test for Path I and using Task 6C model:

$<\tau>$ = 14h

σ_τ = 12.6h

κ = 1.0e-5 $m/h^{1/2}$

θ = 2.56%

k = 13000 m^{-1}.

The same procedure was applied for Path II. The calibrated temporal moments and ψ value are summarized in Table 4-1. The modelled BTC of Amino G acid in CPT-4b test is compared with the measured BTC in Figure 4-2. The estimated values of k and κ are presented in Table 4-3, and it is noted that all combinations of k and κ values in Table 4-3 provide the same result as shown in Figure 4-2.

Path II contains elements of both Structure #19 and the background fracture BG1. It is believed that the background fracture BG1 generally has smaller transmissivity and thus smaller aperture compared to Structure #19. If this assumption holds, the effective k value for Path II would be larger than the estimated k value for Path I. Then all combinations of k and κ from the row marked with green colour and downward in Table 4-3 equally likely. In lack of information concerning the geometrical properties of BG1, we simply choose a value of k = 17000 m^{-1}, and thus κ = 1e-6. The porosity is then obtained as θ = 0.43% by applying Archie's law (Eq. 4-1).

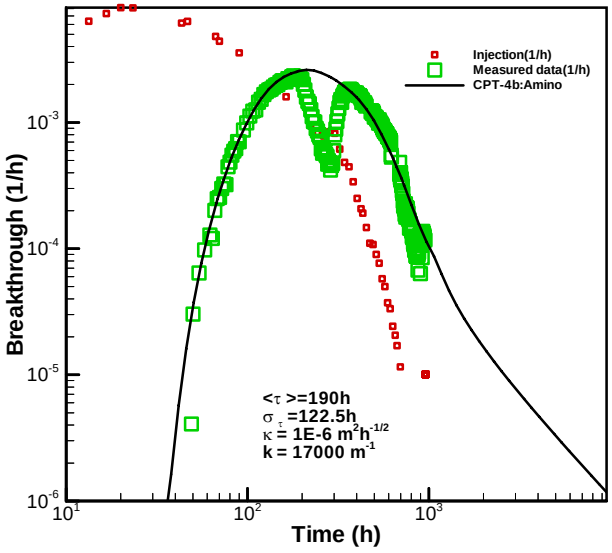

Figure 4-2. *Calibration on the BTC of Amino.G acid in CPT-4b test.*

Table 4-3 Estimation table of k and κ values for kκ = 0.017($h^{-1/2}$), and the corresponding aperture and porosity value for Path II.

k (m^{-1})	Aperture(mm)	κ ($m/h^{1/2}$)	θ(%)
9000	0.22	1.89e-6	0.7
13000	0.15	1.31e-6	0.53
17000	0.12	1e-6	0.43
21000	0.095	8.10e-7	0.36
25000	0.08	6.8e-7	0.32

The calibrated effective parameters on the BTC of Amino G acid in CPT-4b test (Path II) are summarized as follows:

$<\tau>$ = 200 h

σ_τ = 122 h

κ = 1.0e-6 $m/h^{1/2}$

θ = 0.43%

k = 17000 m^{-1}.

These values are applicable to the prediction of sorbing tracer BTCs in the same flow path. In order to predict the sorbing tracer BTCs, we also need values of the effective in-situ sorption coefficients K_d and K_a (Eq. 2-7) which will be discussed in the next section.

4.3 Retention parameters

For Structure #19, the K_a and K_d data were provided for the rim zone as shown in Table 1-1 by Byegård and Tullborg, (2004). The K_d data were also provided for the fault gouge material in Structure #19 (Table 1-1). However no definite conclusion could be drawn with regards to the presence of fault gouge material and its exact amounts. For the task of predicting sorbing tracer BTCs in Path I, we assume here that the "rim zone properties" are representative of effective immobile zone, thus effective K_a and K_d values would be based only on rim zone property of Structure #19 for Path I.

The rim zone in Structure #19 is interpreted to consist of 80% altered rock and 20% of cataclasitic/ mylonitic rock (Byegård and Tullborg, 2004). The sorption coefficients for the two rock types are summarized in Table 1-1.

The effective values are obtained by a simple averaging method. Take the K_d value for Rb-86 as an example. K_d for Rb-86 is $4 \cdot 10^{-4}$ (Table 1-1) for altered zone (80%) and $4 \cdot 10^{-3}$ (also the upper-limit value is taken) for Mylonitic/cataclasitic rock (20%). The effective value for the effective rim zone is therefore calculated as:

$$K_d = 4 * 10^{-4} \times 0.8 + 4 * 10^{-3} \times 0.2 = 1.12 * 10^{-3}$$

The effective K_d values for other tracers and the effective K_a values are obtained by the same procedure and are shown in Table 4-4.

Table 4-4 Summary of predicted effective retention parameters for Path I

Tracer	D_w (m^2/h)	K_d (m^3/kg)	κ (m $h^{-1/2}$)	K_a (m)
Uranine	1.8E-6	0	1.0E-5	0
$^{131}I^-$	7.20E-6	0	2.0e-5	0
$^{160}TbDTPA^{2-}$	1.8E-6	0	1.0E-5	0
$^{85}Sr^{2+}$	2.86E-6	4.9e-5	3.124e-5	1.64e-5
$^{86}Rb^+$,	7.416E-6	1.1e-3	2.2e-4	2.4e-4
$^{137}Cs^+$	7.45E-6	6.4e-3	5.3E-4	2.8E-3

The sorption parameters for the prediction for Path II are also obtained in a similar way as for Path I (Table 4-5).

Table 4-5 Summary of predicted effective retention parameters for Path II

Tracer	D_w (m^2/h)	K_d (m^3/kg)	κ (m $h^{-1/2}$)	K_a (m)
AminoG,	1.8E-6	0	1e-6	0
HTO	7.668E-6	0	2.07e-6	0
$^{155}EuDTPA^{2-}$	1.8E-6	0	1e-6	0
$^{22}Na^+$,	4.788E-6	1.7e-6	2.35e-6	7.0e-7
$^{133}Ba^{2+}$,	3.053E-6	6.9e-4	2.72e-5	2.9e-4
$^{54}Mn^{2+}$	2.477E-6	4.3e-3	6.45e-5	1.8e-3

The fault gouge material is not explicitly accounted for in the predictions, i.e., its effect is incorporated into effective parameters for surface sorption and matrix diffusion.

4.4 Prediction results

The predicted recovery times of 5%, 50% and 95% for the full measured injection source term and for a Dirac pulse injection are summarized in Table 4-6 through Table 4-9. The predicted BTCs are compared with the experimental data in Figure 4-3 and Figure 4-4. The symbols are measured data, while the plotted lines are the predicted BTCs. For Path I, the predicted BTCs generally compare well with the measured data for the conservative tracers. An apparent deviation is observed for tracer Rb-86 (the purple line and symbols). The predicted BTC for Cs-137 also deviates from the measured data (the orange line and symbols), although the deviation is smaller than that for Rb-86.

Table 4-6. Predicted breakthrough times for measured injection in Path I with corresponding measured times in parentheses

Tracer	T_5 (h)	T_{50} (h)	T_{95} (h)	Recovery(%) T=5000h
I-131	16.0 (14)	56.2 (62)	493.7	100
Tb-160	14.88 (14)	48.1 (63)	441.2	100
Sr-85	18.87 (19)	73.31 (107)	1140	100
Rb-86	100.8 (51)	1157 (490)	53600	76
Cs-137	418 (555)	6030	3.1E+5	46

Table 4-7 Breakthrough times for Dirac pulse injection in Path I.

Tracer	T_5 (h)	T_{50} (h)	T_{95} (h)	Recovery(%) T=5000h
I-131	3.56	19.8	463	100
Tb-160	3.14	13.21	135.2	100
Sr-85	4.81	33.7	1100	100
Rb-86	46.93	988	53220	75
Cs-137	323.9	5895	3.1E+5	47

Table 4-8. Predicted breakthrough times for measured injection in Path II with corresponding measured times in parentheses.

Tracer	T_5 (h)	T_{50} (h)	T_{95} (h)	Recovery(%) T=5000 h
HTO	128 (183)	343.5 (790)	2044	100
Eu-155	119.2 (155)	302 (500)	889.3	100
Na-22	124.6 (300)	353 (1490)	2514	100
Ba-133	979.2 (3250)	7758	2.9E+5	40
Mn-54	4844	42730	1.6E+6	5.3

Table 4-9 Breakthrough times for Dirac pulse injection in Path II.

Tracer	T_5 (h)	T_{50} (h)	T_{95} (h)	Recovery(%) T=5000 h
HTO	73.62	226.9	1934	100
Eu-155	68.35	185.4	708.1	100
Na-22	75.83	242.1	2416	100
Ba-133	868.9	7643	2.9E+5	40
Mn-54	4741	42630	1.6E+6	5.6

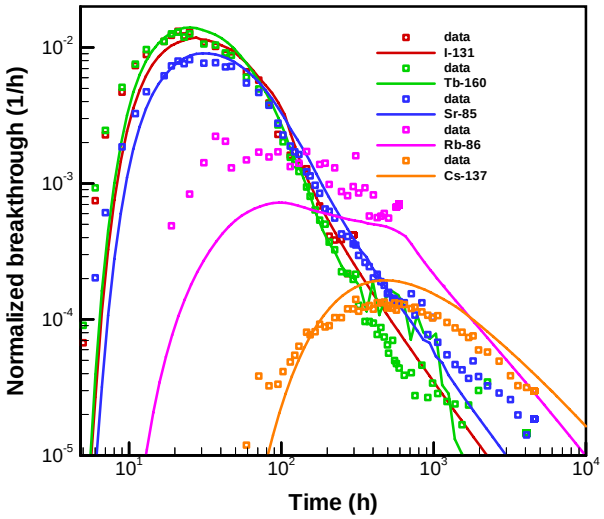

Figure 4-3. *Comparison of predicted and measured BTCs for Path I.*

For path II, the deviations between the predicted BTCs and the measured data are more apparent (for all tracers) and are larger than those for Path I.

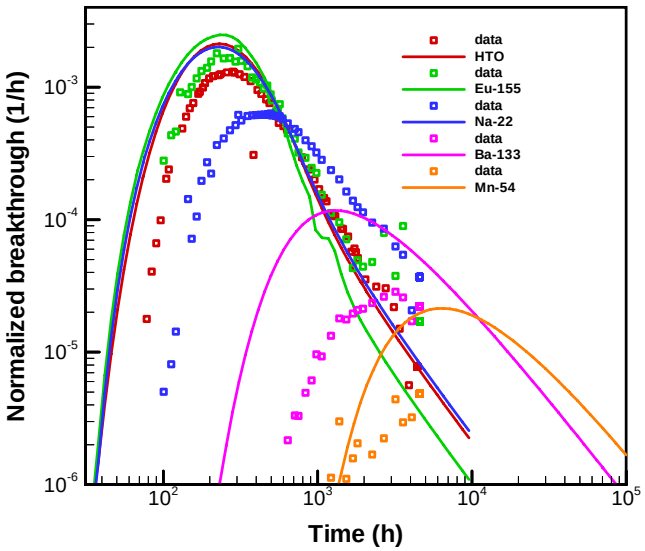

Figure 4-4. *Comparison of predicted and measured BTCs for Path II.*

5 Evaluation using effective retention parameters

In this chapter we present our evaluation results of the BS2B tests in the TRUE Block Scale Continuation project. The objective of this evaluation is to provide estimates of the effective retention parameters by assuming the best fit between measured and modelled BTCs. The model is formulated in a manner as to minimize the number of calibration parameters using the LaSAR framework presented in Chapter 2.

In Path I, four tracers (I-131, Sr-85, Rb-86, Cs-137) were injected and all of them were detected in the pumping borehole with variable mass recoveries (from 28% to more than 80%). In Path II, another four tracers (HTO, Na-22, Ba-133, Mn-54) were injected and all of them were also detected in the pumping borehole with different recoveries. Since the recovery rate for Mn-54 was only about 1%, the evaluation of Mn-54 is not pursued further in this report.

5.1 Evaluation procedure

The evaluation has essentially been carried out in two steps:

- The water residence time distribution $g(\tau)$ is determined by deconvoluting the BTC of I-131 for flow path I (and HTO for flow path II), accounting for diffusion into the matrix. The actual form of $g(\tau)$ is assumed to be inverse-Gaussian, and the first two moments of water residence time are calibrated.
- The $g(\tau)$ is used to model the BTCs of the reactive tracers by accounting for mass transfer processes, with effective parameters determined from the values for the rim zone (see section 4.3). If the modelled BTCs deviate from the observed BTCs, the extent of mass transfer is modified by changing the κ values.

Increasing κ may imply that larger values of the physical parameters θ and/or of the sorption coefficient K_d^m are assumed. The details of the evaluation procedure for the two flow paths are as following:

Path I: KI0025F02:R3(#19) $\rightarrow$ KI0025F03:R3 (#19)

- Fit the experimental BTC of I-131 to obtain $<\tau>$, σ_τ^2, ψ by assuming $\beta = k\tau$,
- k was kept the same as for the prediction (k = 13000 m^{-1}) being in consistency with the effective aperture for Structure #19.
- From the κ thus obtained, back out the porosity θ by assuming Archie's law (Eq. 4-1),
- Assume that the value of θ is applicable for all tracers employed in the flow path,
- Use the K_a values as for the prediction (Table 4-4),Fit the measured BTCs of the sorbing tracers to obtain a κ value for the corresponding tracers,

Path II: KI0025F02:R2(#BG1) → KI0025F03:R3 (#19)

- Fit the experimental BTC of HTO to obtain $<\tau>$, σ_τ^2, ψ by assuming $\beta = k\tau$,
- k was kept the same as for the prediction (k = 17000 m^{-1}),
- From the κ thus obtained, back out the porosity θ by assuming Archie's law (Eq. 4-1),
- Assume that the value of θ is applicable for all tracers employed in the flow path,
- K_a of tracer Ba-133 was kept the same as for the prediction (Table 4-5), K_a of tracer Na-22 was obtained by fitting the measured BTC,
- Fit the measured BTCs of the sorbing tracers to obtain a κ value for the corresponding tracers,
- The tracer Mn-54 was not evaluated due to low mass recovery and very few measured data.

5.2 Retention parameters

For Path I

The evaluated parameters obtained from the measured BTCs are summarised in Table 5-1. The calibrated temporal moments from the I-131 data are $<\tau>$ = 12 h and σ_τ^2 =200 h^2 . The slope *k* is 13000 m^{-1} (Table 5-3). The rock density ρ is 2700 kg/m^3.

Table 5-1. Summary of the sorption and diffusion parameters for Path I.

Tracer	D_w (m^2/h)	K_d (m^3/kg)	θ (%)*	κ (m $h^{-1/2}$)	K_a (m)
I-131	7.20E-6	0	2.6	2.0e-5	0
Sr-85	2.86E-6	1.4e-4	2.6	5.0e-5	1.64e-5
Rb-86	7.416E-6	5.0e-4	2.6	1.5e-4	2.4e-4
Cs-137	7.45E-6	2.6e-2	2.6	1.1e-3	2.8E-3

For Path II

The evaluated parameters obtained from the measured BTCs are summarised in Table 5-2. The calibrated temporal moments from the HTO data are $<\tau>$ = 270 h and σ_τ^2 = 25000 h^2 . The slope *k* is 17000 m^{-1} (Table 5-3). The rock density θ is 2700 kg/m^3.

Table 5-2. Summary of the evaluated sorption and diffusion parameters for Path II.

Tracer	D_w (m^2/h)	K_d (m^3/kg)	θ (%)	κ (m $h^{-1/2}$)	K_a (m)
HTO	7.668E-6	0	0.42	2.0e-6	0
Na-22	4.788E-6	2.1e-5	0.42	6.0e-6	7.0e-7*40
Ba-133	3.053E-6	2.1e-3	0.42	4.7e-5	2.9e-4

Table 5-3. Summary of flow dependent parameters from evaluation.

Path	$<\tau>$ (h)	σ_τ^2 (h^2)	k (m^{-1})	$<\beta>$ (hm^{-1})
I: KI0025F02:R3(#19) → KI0025F03:R3 (#19)	12	200	13000	1.56E+5
II: KI0025F02:R2(#25) → KI0025F03:R3 (#19)	270	25000	17000	4.59E+6

5.3 Evaluation results

The evaluated BTCs are compared with the measured data for Path I in Figure 5-1. The lines are the evaluated BTCs, while the symbols are the measured data.

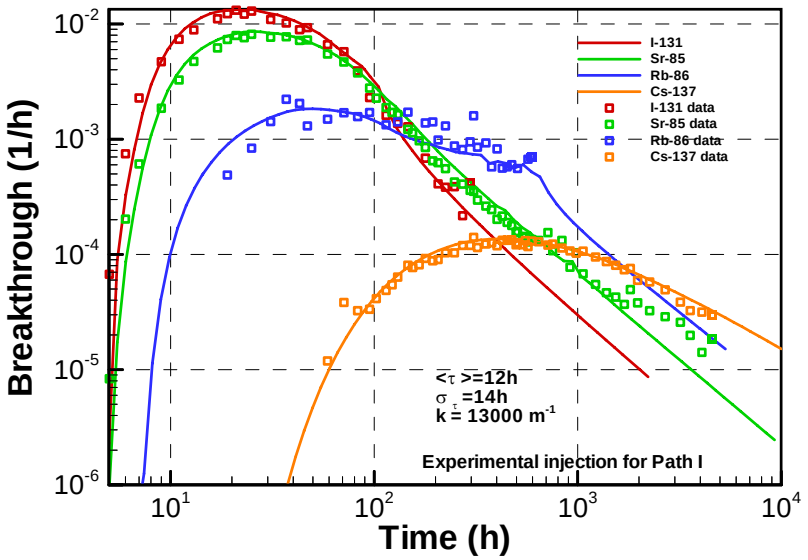

Figure 5-1. *Evaluated BTCs compared with the experimental data for Path I.*

Table 5-4. Evaluated breakthrough times for the measured injection in Path I with corresponding measured times in parentheses.

Tracer	T_5 (h)	T_{50} (h)	T_{95} (h)	Recovery (%) T=5000 h
I-131	13.21 (14)	48.33 (62)	375.4	100
Sr-85	16.75 (19)	78.7 (107)	2026	98
Rb-86	44.9 (51)	517.7 (490)	1.91e+4	86
Cs-137	475.4 (555)	13190	9.55e+5	35

The evaluated BTCs are compared with the measured data for Path II in Figure 5-2. The lines are the evaluated BTCs, while the symbols are the measured data.

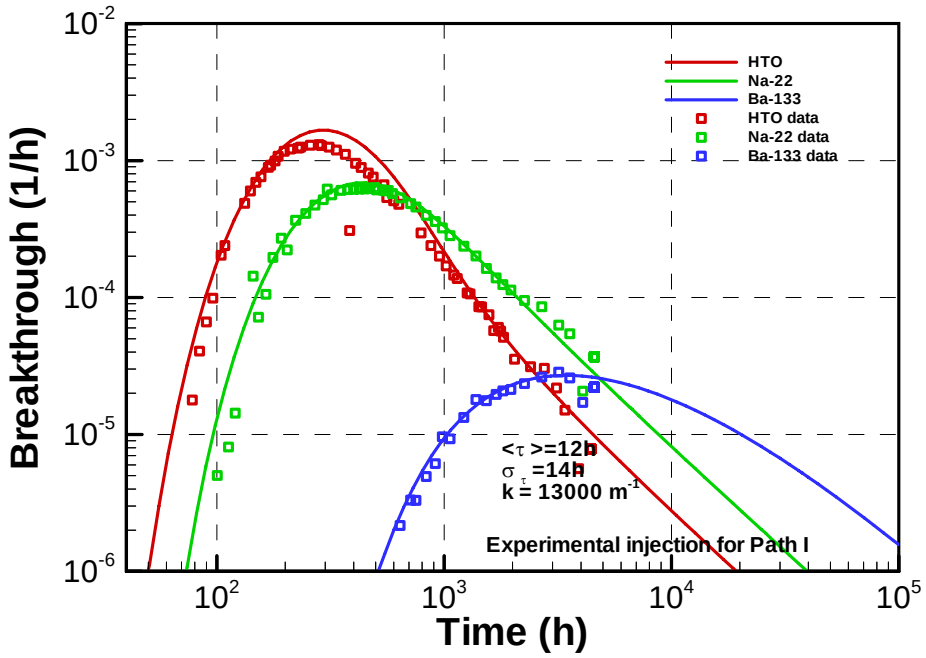

Figure 5-2. *Evaluated BTCs compared with the experimental data for Path II.*

Table 5-5. Evaluated breakthrough times for measured injection in Path II with corresponding measured times in parentheses.

Tracer	***T_5* (h)**	***T_{50} (h)***	***T_{95} (h)***	***Recovery (%) T=5000 h***
HTO	166.9 (183)	444.5 (790)	3292	97
Na-22	274 (300)	1090 (1490)	26110	82
Ba-133	2945 (3250)	37650	1.57e+6	11
Mn-54	-	-	-	

6 Accounting for heterogeneity of retention parameters

Retention parameters on the field scale are in general spatially variable. Both the porosity θ and the sorption coefficient K_d may vary longitudinal (i.e., in the x-y plane as the tracer particles move along the flow path), as well as depth-wise (i.e., in the z-direction, normal to the fracture plane) as the particles diffuse into the rock matrix. In the Task 6C model (Dershowitz et al., 2003), two structure types were defined to account for the depth-wise variability of θ and K_d into the rock matrix. In this chapter we shall use the definition of the two structure types in the Task 6C model to account for the depth dependence of θ and K_d. We shall estimate the penetration depths for individual tracers, and then obtain the effective values of θ and K_d based on the penetration depths for each tracer. We shall also compare the parameters with those obtained from the calibration procedure in Chapter 5.

6.1 Microstructural model

A semi-synthetic hydro-structural model was developed in Task 6C for the TRUE Block Scale test site (Dershowitz et al., 2003). Two basic structure types were defined in the Task 6C model: structure Type 1 (fault) which consists of five parallel retention (or immobile) zones; fracture coating, fault gouge, cataclasite, altered zone and intact rock (Figure 2-2 in Dershowitz et al., 2003), and structure Type 2 (non-fault) which simply consists of the fracture coating, the altered rock and the intact rock (Figure 2-3 in Dershowitz et al., 2003).

The two types (1 and 2) of the geological structures are quantified in terms of the thickness and porosity (as well the formation factor) of each geologically defined retention zone shown in Table 2-1 and Table 2-2 in Dershowitz et al., 2003.

For the purpose of TRUE Block Scale Continuation project, Type 1 and Type 2 structures are being defined in consistency with those in the Task 6C model (Dershowitz et al., 2003), with some modifications of the thickness of the retention zones (Tullborg and Hermanson, 2004) and distribution of the retention zones.

The microstructural models for Geological Structures (Type 1 and Type 2) are quantified in terms of the thickness of each of the geometrically defined (retention) zones, and the porosity and formation factor of those zones. Since both Type 1 and Type 2 structures can be made up of multiple discrete features, the representative thickness provided for each of the zones is per feature. Larger structures tend to be made up of more features, and will consequently have a greater total thickness of each zone. In addition, the thickness of each zone can be scale-dependent. The properties of the Geological Structures Type 1 and Type 2 are provided in Table 6-1 and Table 6-2, respectively (Tullborg and Hermanson, 2004).

Table 6-1 Properties of geological structure Type 1 for BS2B evaluation (Tullborg and Hermanson, 2004).

Rock type	Thickness (cm)	Porosity (%)	Formation factor (−)
Intact wall rock	−	0.3	7.3E-5
Altered zone	15	0.6	2.2E-4
Cataclasite/Mylonite d_{cm}	1	1	4.9E-4
Fault gouge d_g	0.3	20	5.6E-2
Fracture coating d_c	0.05	5	6.2E-3

Table 6-2. Properties of geological structure Type 2 for BS2B evaluation (Tullborg and Hermanson, 2004).

Rock type	Extent (cm)	Porosity (%)	Formation factor (−)
Intact wall rock	−	0.3	7.3E-5
Altered zone	5	0.6	2.2E-4
Fracture coating d_c	0.05	5	6.2E-3

Compared with the Task 6C model (Table 2-1 and 2-2 in Dershowitz et al., 2003), the retention zones in BS2B model (Table 6-1 and 6-2) are thinner for all zones, except for fracture coating.

In Dershowitz et al. (2003) the sorption coefficient K_a for the fracture surface is calculated from the K_d values of the thin fracture coating. *The fracture coating is therefore considered as the fracture surface in our calculation*. The 0.05 cm thick fracture coating is assumed to be evenly distributed on both sides of the fracture, i.e., 0.025 cm on each side (Figures 6-1 and 6-2). This assumption is applicable for both types of the structures.

For structure Type 2 there is a 5cm altered zone behind the fracture coating. It is also assumed that the altered zone is evenly distributed on both sides of the fracture adjacent to the rock matrix, i.e., 2.5cm on each side. Outside the altered zone is the intact rock matrix (Figure 6-1).

Table 6-3 summarizes the porosity profile for structure Type 2 at different depths in the rock matrix. The porosity is generally decreasing with depth into the rock matrix.

Table 6-3. Porosity profile at different depths for structure Type 2 (Tullborg and Hermanson, 2004)..

Rock type	Depth (mm)	Porosity (-)
Fracture coating	0 – 0.25	0.05
Altered zone	0.25 – 25.25	0.006
Unaltered	25.25 -	0.003

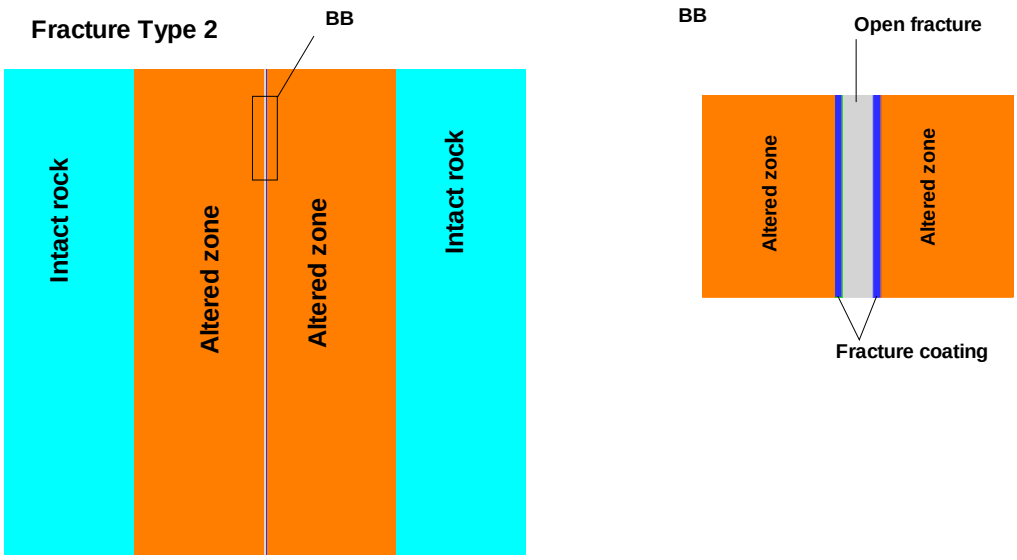

Figure 6-1 *Distribution of the retention zones in structure Type 2. Fracture coating is viewed as fracture surface.*

For structure Type 1 the situation is more complicated. The thin fracture coating is still assumed to be evenly distributed on both sides of the fracture. Two other zones (the cataclasite and the fault gouge zones) are behind the fracture coating in the microstructural model of Type 1 structure. The structure shown in Figure 2-1 in Dershowitz et al., 2003 should be considered as to be somehow arbitrary since it is unlikely in reality that the cataclasite is always on one side of the fracture while the fault gouge on the other side. In reality it is more likely that at some points the cataclasite is on one side while at other points it is on the other side. The same is true for the fault gouge. They will be irregularly distributed on both sides of the fracture. In lack of detailed information concerning their distribution we assume that of the cataclasite is distributed along 50% of the length of the flow path and the fault gouge along the other 50% of the length. However, in this report they are not assumed to be monotonously distributed along respective sides of the fracture, but alternatively distributed on both sides as is shown in Figure 6-2. The altered zone (7.5 cm thick) is still evenly distributed on both sides of the rock matrix. The intact rock zone is behind the altered zone on both sides (not shown in Figure 6-2).

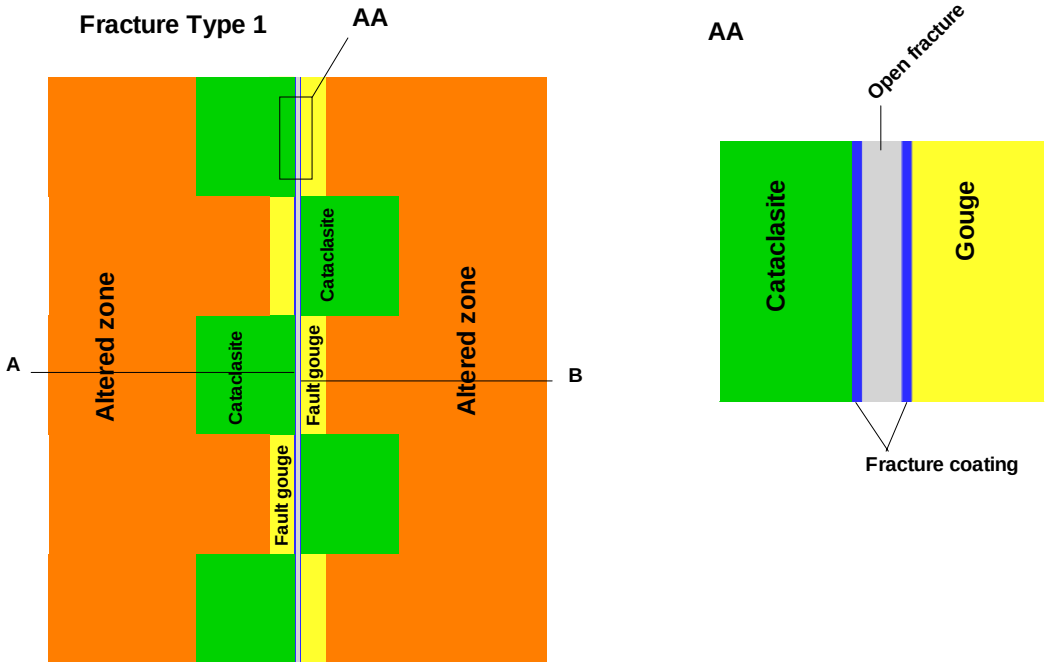

Figure 6-2. *Distribution of the retention zones in structure Type 1. Part A: Cataclasite+altered zone +intact rock. Part B:Fault gouge+ altered zone +intact rock Fracture coating is viewed as fracture surface.*

As is shown in Figure 6-2, the immobile zone in structure Type 1 is divided into two parts in terms of different retention zones on two sides of open fracture. In the middle lies the open fracture with the fracture coatings. The fracture coatings/sections are treated as the fracture surface. The first part of the immobile zone (part A in Figure 6-2) contains the following retention zones: the cataclasite, the altered zone and the intact rock. The second part (part B in Figure 6-2) contains the retention zones of the fault gouge, the altered zone and the intact rock. For surface sorption coefficient K_a, we take the values suggested by (Tullborg and Hermanson, 2004). The fracture surface is not part of the immobile zone, but considered as to be equivalent to fracture coating in Figure 6-2. The other retention zones, including the cataclasite, the altered zone and the (unaltered) intact rock zone, constitute the rock matrix in Part A. It is assumed that these three zones are evenly distributed on both sides of the fracture. From the data shown in Table 6-1 the porosity profile at different depths within the rock matrix is given by Table 6-4 and Table 6-5.

Table 6-4. Porosity profile at different depths within the immobile zone for structure Type 1, Part A in Figure 6-3.

Rock type	Depth (mm)	Porosity
Fracture coatings	0 – 0.25	0.05
Cataclasite	0.25 – 10.25	0.01
Altered zone	10.25 – 85.25	0.006
Intact rock	85.25 -	0.003

Table 6-5. Porosity profile in depth for structure Type 1 for Part B in Figure 6-3

Rock type	Depth (mm)	Porosity
Fracture coatings	0 – 0.25	0.05
Fault gouge	0.25 – 3.25	0.20
Altered zone	3.25 – 78.25	0.006
Intact rock	78.25 -	0.003

The fracture coating is in immediate contact with the groundwater, and is to be viewed as the fracture surface (K_a). Our main task is then to estimate effective θ and K_d values for effective immobile zone.

Diffusivity

Given the formation factor *F*, the effective diffusivity is calculated by $D_e = D_w \cdot F$ where D_w ($L^2\ T^{-1}$) is the diffusivity of the tracer in bulk water. The calculated D_e values for different tracers in contact with different rock materials are listed in Table 6-6 (Byegård and Tullborg, 2004).

Table 6-6. Effective diffusivities for different tracers in contact with different rock materials (from Byegård and Tullborg, 2004). The diffusivities have been calculated using the formation factor, F, and the tabulated water diffusivities, D_w.

		Fracture Coating (BG1)	Fault Gouge (#19)	Cataclasite (#19)	Altered Zone (#19 and BG1)
	Porosity (%)	5	20	1	0.6
	Formation factor	6.2E-3	5.6E-2	4.9E-4	2.2E-4
Tracer	D_w (m^2/s)	D_e (m^2/s)	D_e (m^2/s)	D_e (m^2/s)	D_e (m^2/s)
$^{131}I^-$	2.00E-9	1.2E-11	1.1E-10	9.8E-13	4.4E-13
HTO	2.13E-9	1.3E-11	1.2E-10	1.0E-12	4.7E-13
$^{22}Na^+$	1.33E-9	8.3E-12	7.4E-11	6.5E-13	2.9E-13
$^{85}Sr^{2+}$	7.94E-10	5.0E-12	4.4E-11	3.9E-13	1.7E-13
$^{86}Rb^+$	2.06E-9	1.3E-11	1.2E-10	1.0E-12	4.5E-13
$^{137}Cs^+$	2.06E-7	1.3E-11	1.2E-10	1.0E-12	4.5E-13
$^{133}Ba^{2+}$	8.48E-10	5.3E-12	4.7E-11	4.2E-13	1.9E-13
$^{54}Mn^{2+}$	6.88E-10	4.3E-12	3.8E-11	3.4E-13	1.5E-13

6.2 Fracture rim zone

From the laboratory program, the rim zone material of Structure #19 consists of approximately 80% of “strongly hydrothermally altered rock” and to 20% of “mylonitic and cataclasitic wall rock, in Äspö diorite” (Byegård and Tullborg, 2004). The fault gouge material also exists in Structure #19 from the laboratory experiments (Byegård and Tullborg, 2004). Structure #19 is considered as a Type 1 structure. In the definition of the Type 1 structure, the retention zones include the gouge material, the cataclasite, and the altered rock which are consistent with the composition of the rim zone material and the

gouge material of the laboratory experiments. We therefore assume the K_d values of the tracers in Path 1 presented in Table 1-1 are also applicable for the corresponding retention zones in the microstructural model of the Type 1 structure (Table 6-7).

The rim zone material of BG1, defined from the laboratory experiments, is the altered Äspö diorite which is consistent with the the Type 2 structure of the microstructural model. We therefore assume the K_d data of the rim zone material of BG1 are valid for the altered rock in the Type 2 structure (Table 6-7).

The K_d values are summarized in Table 6-7. Note that these K_d values may differ from the values given in Task 6C (c.f. Table 2-6 in Dershowitz et al., 2003). There are no data available for intact rock material in /Byegård and Tullborg, 2004/. The K_d data provided in the Task 6C model (Dershowitz et al., 2003) are larger than the K_d values for the altered zone as is shown in Table 6-7. which is unlikely. We therefore assume that the intact rock has the same K_d values as that for the altered zone shown in Table 6-7. The K_d data for the intact rock may also be obtained from the MIDS data of the TRUE-1 project (Byegård et al., 1998). However this will probably not affect the final results.

The rim zone material in the laboratory experiments is considered in terms of composition, the spatial distribution of the material is not accounted for. We take into account the spatial distribution as shown in Figures 6-1 and 6-2 (Tullborg and Hermanson, 2004), and consider the depth-dependent variability as well.

By using the definition of two structure types in spatial distribution and assign the retention properties from the laboratory data, we relate the microstructural model with the laboratory data and the definition of rim zone.

Table 6-7. Summary of the K_d values for different rock materials in contact with the TRUE Block Scale groundwater (Byegård and Tullborg, 2004).

Tracer	Structure	Gouge	Cataclasite	Altered zone	Intact rock
		θ=0.2 K_d (m^3/kg)	θ=0.01 K_d (m^3/kg)	θ=0.006 K_d (m3/kg)	θ=0.003 K_d (m3/kg)
$^{85}Sr^{2+}$	#19	6.0e-4	1.4e-4	2.6e-5	2.6e-5
$^{86}Rb^{+}$	#19	2.7e-3	4e-3	4e-4	4e-4
$^{137}Cs^{+}$	#19	4.0e-2	3e-2	5e-4	5e-4
$^{22}Na^{+}$	BG1	-	-	1.7e-6	1.7e-6
$^{133}Ba^{2+}$	BG1	-	-	6.9e-4	6.9e-4
$^{54}Mn^{2+}$	BG1	-	-	4.3e-3	4.3e-3

**The density ρ is assumed to be 2700kg/m^3 for all zones.*

6.3 Depth-dependent variability

In this section, we shall estimate the penetration depth for individual tracers, and then estimate effective values of θ and K_d based the penetration depths and on the data in Table 6-4 to Table 6-7.

The governing equation for the concentration profile in the rock matrix is (the advection in the matrix is neglected):

$$\frac{\partial C}{\partial t} = \frac{\partial}{\partial z}\left[\frac{D_p}{R}\left(\frac{\partial C}{\partial z}\right)\right] \qquad (6\text{-}1)$$

where $R = 1 + \frac{K_d \rho}{\theta}$ is the retardation factor. The boundary condition is specified at the fracture surface as $C(0, t)$ which is the tracer concentration in the fracture. The two parameters, D_p and R determine the concentration in the rock matrix.

Using (Eq. 4-1) and from the relation $D_p = FD_w$, the pore diffusivity D_p can be expressed as:

$$D_p = 0.71\theta^{1.58} D_w \qquad (6\text{-}2)$$

The pore diffusivity then depends on the porosity θ that varies with depth into the rock matrix.

The retardation factor R is also depth-dependent since it depends on θ and K_d.

For a given retention zone, Equation (6-1) has the solution (D_p and R assumed constant):

$$C(z,t)/C_0 = C'(z,t) = \left(1 - erf\,\frac{z}{\sqrt{4D_p t/R}}\right) \qquad (6\text{-}3)$$

The equation shows that the normalized concentration depends on time t and the penetration depth z.

The immobile zone for both types of structures consists of several parallel retention zones (Figure 6-1, 6-2). Equation (6-3) is applicable for individual layered zones, while different zones may have different retention parameters. We have to calculate the concentration $C(z, t)$ zone by zone in succession. The concentration obtained at the end boundary of a previous zone will serve as the initial concentration for the subsequent zone, and so on. The retention zone presented in this chapter may or may not be the same as the rim zone presented in Chapter 5. Depending on the penetration depth, the rim zone may consist of one or several different retention zones.

The penetration profile $C(t, z)$ (Eq. 6-3) can be estimated as a function of depth z at a specified time t. The time should be that when most of the mass has been recovered, and after which the penetration slows down significantly. The highest mass recoveries for tracers in Path I, as summarized in Table 3-2, are between 80% and 86%. We therefore choose the time at which 85% mass recovery is recovered for estimating penetration depths. We also need to specify a relative concentration C/C_0 to define an "effective" depth z. As a cut-off for defining the penetration depth we choose the relative concentration $C/C_0 = 0.15$; at approximately this value the first derivative with respect to z is significantly reduced whereby the profile curves start a relatively slow convergence to zero. Thus for $C/C_0 > 0.15$ we capture the bulk of the penetrated mass and consider this appropriate for obtaining an effective porosity.

Equation (6-3) is strictly valid only for constant parameters D, R and constant C_0 in open fractures. We have concentrations (or BTCs) varying with time in the fracture. Cvetkovic and Cheng (2002) have compared the concentration profiles obtained numerically with time-varying boundary conditions (proportional to the breakthrough curve), with profiles obtained from Equation (6-3). It was found that Equation (6-3) provides a reasonable approximation. Given all uncertainties in the system, we consider Equation (6-3) as a reasonable approximation for estimating the penetration profiles which are used for averaging/inferring an "effective" porosity and K_d.

6.3.1 Path I

Our aim is to find out the effective values of the retention parameters (θ and K_d) along the flow path for the tracers by accounting for the depth heterogeneity and compare them with the parameters obtained from the evaluation based on the calibration procedure in Chapter 5. The following is the calculation procedure:

- Obtain times for 85% recovery for every tracer from the evaluated BTCs in Chapter 5 for Path I;
- Use the obtained times to calculate penetration depths for the tracers into two structure types (as Path I contains both Type 1 and Type 2 structures as shown in Table 6-4);
- Find the depths where $C(z, t)/C_0 = 0.15$;
- Use the depths to calculate the effective θ and K_d;Average results over the structure types.
- Compare the obtained K_d and θ with the ones obtained from the evaluation in Chapter 5 (Table 5-1).

The 85% recovery times are shown in the last column of Table 6-8 as obtained from the evaluated BTCs (Figure 5-1).

Table 6-8. Times for 85% mass recovery for Path I.

Tracer	D_w (m^2/h)	T (h) (85%)
I-131	7.20E-6	126
Sr-85	2.86E-6	506.4
Rb-86	7.416E-6	4254
Cs-137	7.45E-6	210200

For structure Type 1 calculations of the penetration profiles should be performed separately for the two parts of the immobile zone (Part A and Part B in Figure 6-2). The Part A section includes the cataclasite zone, the altered zone and the intact rock. The Part B section consists of the fault gouge zone, the altered zone and the intact rock. In the Part A section the tracers diffuse into the cataclasite zone and probably also into the altered zone and the intact rock matrix. In the Part B section tracers first diffuse into the fault gouge zone, then into the altered zone and subsequently into the intact rock matrix.

We let the time *t* (Eq. 6-3) to be the 85% recovery time shown in Table 6-12 and use other parameter values for the corresponding layers as shown in Table 6-11 to calculate the normalized concentration (Eq. 6-3) as a function of the penetration depth z. We obtain the penetration profiles for the Part A section (Figure 6-3a) and for the Part B section (Figure 6-3b).

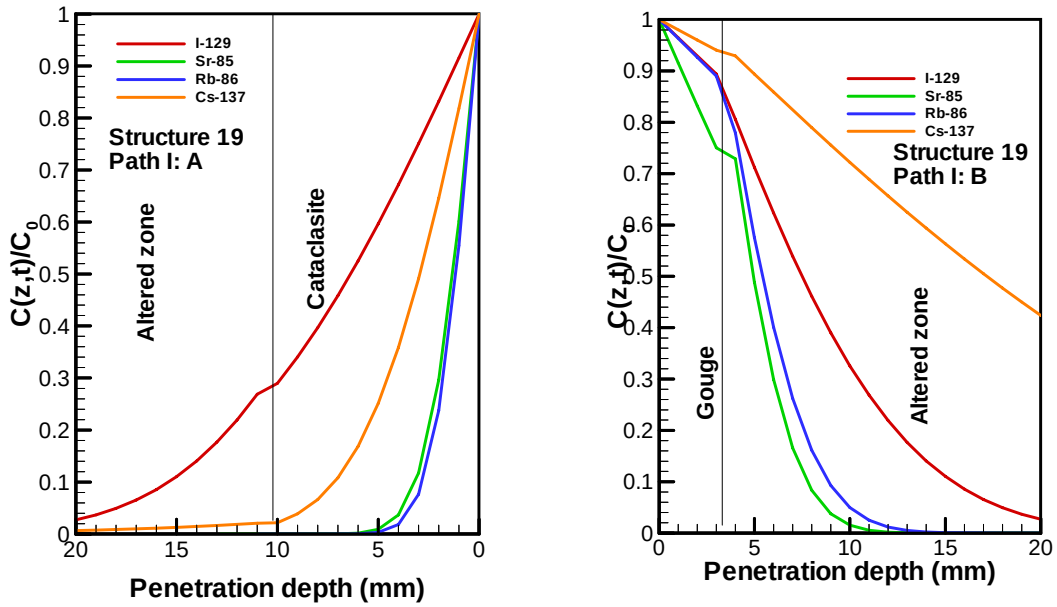

Figure 6-3. *Penetration profile. (a) for Part A section (b) for Part B section in structure Type 1 (Figure 6-2). The profiles are calculated at the times of 85% mass recovery. The times are 126 h for I-131, 506 h for Sr-85, 4254 h for Rb-86, $2.1 \cdot 10^5$ h for Cs-137.*

If C/C_0 = 15% is chosen as a limit of penetration we get the penetration depths for the two parts of the immobile zone in structure Type 1 that are shown in Table 6-13. The effective values of θ and K_d in Tables 6-9 and 6-10 are calculated based on the penetration depth.

From Table 6-9 we find that the penetration depths of the tracers vary. For the structure Type 2, all tracers penetrate into the altered zone, with penetration depths from a few millimetres to tens of millimetres. For the two parts of the immobile zone in structure Type 1, the penetration depths range from 3 mm to more than 30 mm.

Our aim is to find one single effective value of θ and K_d for each tracer over the effective immobile zone and compare the values with those obtained from the evaluation in Chapter 5. A simple depth-weighted average value will first be used to obtain the effective value of θ for each tracer. The same type of average value is also obtained for K_d. Take I-131 in structure Type 1 as an example. I-131 penetrates totally 14 mm into the rock matrix on both sides of the fracture zone for Type 1 fracture. For the combination of the cataclasite, and the altered zone, it penetrates 14 mm. The first 10 mm is in the cataclasite and the remaining 4 mm is in the altered zone. An effective θ is then calculated as:

$$\theta_e = \frac{10}{14} \times 1\% + \frac{4}{14} \times 0.6\% = 0.9\%$$

We thus have an effective porosity of 0.9% for I-131 for the part A of the structure Type 1. For the part B (the fault gouge, the altered zone and the intact rock) of the structure Type 1, I-131 penetrates the first 3 mm in the fault gouge, and the remaining 11 mm in the altered zone. The total depth is 14 mm. Based on these data, an effective porosity of 4.8% is obtained for I-131 in the part B of structure Type 1 as shown in:

$$\theta_e = \frac{3}{14} \times 20\% + \frac{11}{14} \times 0.6\% = 4.8\%$$

Each of the Part A and Part B sections of the immobile zone in Structure Type 1 contributes 50% to the effective immobile zone. The effective porosities for the entire structure Type 1 are the averages of the values in the two parts.

The effective porosities thus calculated for the entire Path I for all the tracers are shown in the last column in Table 6-9.

The sorption distribution coefficient K_d is also calculated by the same weighing method. The calculated effective K_d values for the entire path I are presented in Table 6-10.

Table 6-9. Penetration depths at 15% relative concentration of different tracers in Path I and calculated porosities based on the depths.

Tracer	**Type1 (Part A)**		**Type1 (Part B)**		***Effective value***
	Depth (mm)	θ (%)	Depth (mm)	θ (%)	θ (%)
I-129	14	0.9	14	4.8	2.9
Sr-85	3	1	7	8.9	5.0
Rb-86	3	1	8	7.9	4.5
Cs-137	6	1	34	2.3	1.7

Table 6-10. Penetration depths at 15% relative concentration of different tracers in Path I and calculated K_d values based on the depths.

Tracer	**Type1 (Part A)**		**Type1 (Part B)**		***Effective value***
	Depth (mm)	K_d (m^3/kg)	Depth (mm)	K_d (m^3/kg)	K_d (m^3/kg)
I-129	14	0	14	0	0
Sr-85	3	1.4e-4	7	2.7e-4	2.1e-4
Rb-86	3	4.0e-3	8	1.3e-3	2.7e-3
Cs-137	6	3.0e-2	34	4.0e-3	1.7e-2

We have obtained the effective porosities, θ, and the effective K_d values for all tracers, Table 6-15 presents the values of the κ obtained from the effective θ and K_d values. The κ values obtained from the penetration depth are compared also with the evaluated values from Chapter 5 in Table 6-15.

Table 6-11. Comparison of effective retention parameters from penetration calculation and those from evaluation in Chapter 5.

Tracer	Estimate 2 (from penetration depth)			Estimate 1 (from evaluation in Chapter 5)			*Ratio for κ* (Estimate 2/estimate 1)
	θ(%)	K_d (m^3/kg)	κ (m $h^{-1/2}$)	θ(%)	K_d (m^3/kg)	κ (m $h^{-1/2}$)	
I-131	2.9	0	2.2e-5	2.6	0	2.0e-5	1.1
Sr-85	5.0	2.1e-4	1.1e-4	2.6	1.4e-4	5.0e-5	2.2
Rb-86	4.5	2.7e-3	5.4e-4	2.6	5.0e-4	1.5e-4	3.6
Cs-137	1.7	1.7e-2	6.2e-4	2.6	2.6e-2	1.1e-3	0.6

For I-131, the κ values in Estimate 2 are about 10% larger than those in Estimate 1 due to a larger θ value in Estimate 2. For Cs-137, the κ values in Estimate 2 are about 40% smaller than those in Estimate 1 since both the values of θ and K_d are smaller in Estimate 2. While for Sr-85, the κ values in Estimate 2 are approximately a factor 2 of those in Estimate 1 due to a larger θ and K_d value in Estimate 2. For Rb-86, the κ values in Estimate 2 are a factor of 3 of the value in Estimate 1 since there are larger θ and K_d values in Estimate 2.

6.3.2 Path II

Flow path II begins in background fracture BG1 and ends in Structure #19 in the same pumping section as for Path I. It is not clear how the complete flow path is distributed between Structure #19 and BG1, or fractures in between. However the mean travel time in Flow path II evaluated from Chapter 5 is 270 h which is more than an order of magnitude longer than the mean travel time of 12 h in Flow path I (Table 5-3). This suggests that the tracers may spend most time in BG1 (and possibly in additional equitable fractures). In lack of accurate information, we perform the penetration analysis for flow path II based on properties of BG1 alone neglecting Structure #19, and possible intermediate background fractures. Since BG1 is a Type 2 structure, its immobile zone includes altered zone and intact rock. The sorption coefficient K_d for various tracers and the porosities are provided in Table 6-7.

The following procedure was followed in this penetration analysis:

- Obtain times for 85% recovery for every tracer from the evaluated BTCs for flow path II. We also used the time for 85% recovery as for Path I.
- Use the obtained times to calculate penetration depths for the tracers into structure Type 2, and assume the times valid for Path II;
- Find the depths where $C(z, t)/C_0 = 0.15$;
- Use the depths to calculate the effective θ and K_d;Compare the obtained K_d and θ with the ones obtained from the evaluation (Table 5-2).

The 85% recovery times from the evaluated BTCs (Figure 5-2) are shown in the last column of Table 6-16.

Table 6-12. Times for 85% mass recovery for Path II as obtained from BTCs in Figure 5-2.

Tracer	D_w (m^2/h)	T (h) (85%)
HTO	7.67E-6	1162
Na-22	4.79E-6	6708
Ba-133	3.05E-6	377100

For structure Type 2, the structures are relatively simple. The altered zone and the intact rock constitute the rock matrix. The altered zone is evenly distributed in a thickness of 25 mm on both sides of the fracture. In our calculations, the structures are assumed to be symmetric to the fracture plane (Figure 6-1).

The penetration calculation will be performed only on one side. For the reason of symmetry the same results will be valid on the other side. Figure 6-6 shows the penetration profile for the background fracture BG1. All tracers penetrate through the altered zone and into the intact rock.

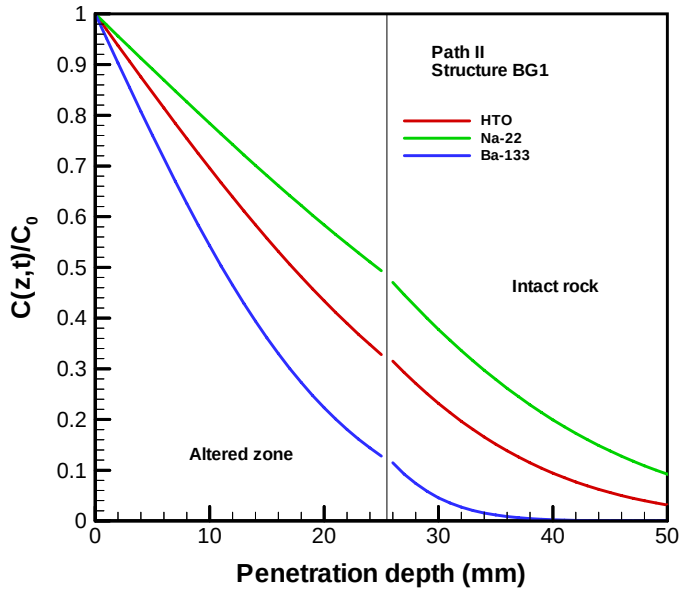

Figure 6-4. *Penetration profiles in the altered zone and the intact rock in background fracture BG1 (Type 2). The profiles are calculated at the times of 85% mass recovery. The times are 1162 h for HTO, 6708 h for Na-22, 377100 h for Ba-133.*

The penetration depths at $C(z,t)/C_0$ =0.15 are presented in Table 6-17. The effective porosity, K_d and κ parameters estimated for Path II from the penetration depths are also shown in Table 6-17.

Table 6-13. Penetration depths at 15% relative concentration of different tracers for Path II represented by background fracture BG1 (Type 2) and the calculated effective retention parameters based on the depths.

Tracer	Path II (Type2)			
	Depth (mm)	θ (%)	K_d (m^3/kg)	κ (m $h^{-1/2}$)
HTO	35	0.51	0	2.6e-6
Na-22	44	0.47	1.7e-6	2.6e-6
Ba-133	24	0.55	6.9e-4	3.3e-5

The retention parameters obtained from the penetration depths are compared also with the evaluated values from Chapter 5 in the Table 6-18.

Table 6-14. Comparison of the effective retention parameters from penetration analysis and those from evaluation in Chapter 5

Tracer	Estimate 2 (from penetration depth)			Estimate 1(from evaluation in Chapter 5)			Ratio of (Estimate 2 / estimate 1)
	θ (%)	K_d (m3/kg)	κ (m $h^{-1/2}$)	θ (%)	K_d (m^3/kg)	κ (m $h^{-1/2}$)	
HTO	0.51	0	2.6e-6	0.42	0	2.0e-6	1.3
Na-22	0.47	1.7e-6	2.6e-6	0.42	2.1e-5	6.0e-6	0.43
Ba-133	0.55	6.9e-4	3.3e-5	0.42	2.1e-3	4.7e-5	0.7

If the κ values of the Estimate 1 in Chapter 5 are considered to be correct, then the κ values in Estimate 2 obtained from the penetration depth are overestimated for the conservative tracer HTO, and are underestimated for the sorbing tracers Na-22 and Ba-133. Although Path II contains Structure #19 and BG1 (or even additional fractures in between), in Estimate 2 only BG1 has been accounted for and Structure #19 has been neglected in the penetration analysis. Exclusion of Structure #19 may therefore be the reason for the underestimation of the κ values for the sorbing tracers.

7 Discussion

7.1 Individual tracers

In the following we will discuss the evaluation results tracer by tracer. We first start with the results obtained for Path I.

7.1.1 Path I

In Figure 7-1, the evaluated BTCs for all tracers in Path I are compared with the predicted BTCs and the measured data relative to the associated non-sorbing conservative tracer.

The initial part of the predicted BTC for conservative tracer I-131 is shifted to the right, indicating that the mean residence time may have been overestimated and the dispersion (due to distribution of τ) underestimated. By decreasing the mean residence time from 14 h (prediction) to 12h (evaluation) and increasing the variance of residence time from 160 h^2 to 200 h^2, the evaluation curve matches well the measured data of I-131 (Figure 5-1). During the fitting, the value of the κ parameter obtained from prediction was kept unchanged.

For Sr-85, the peak of predicted BTC is slightly higher than the measured data, and the tail part of the predicted BTC is lower than the measured data, indicating an underestimate of the retention in the rock matrix. In the evaluation, the value of the κ parameter was increased from $3.1 \cdot 10^{-5}$ m $h^{-1/2}$ (prediction) to $5 \cdot 10^{-5}$ m $h^{-1/2}$ (evaluation), an increase of about 60%. As it has been assumed a constant porosity, an increase of κ implies an increase of the sorption coefficient K_d.

For Cs-137, the deviation of the predicted BTC to the measured data is similar to that of Sr-85, but to a much larger extent. The predicted BTC is obviously higher than the measured data. There is an underestimate of the retention in the matrix. By increasing the value of κ from $5.3 \cdot 10^{-4}$ m $h^{-1/2}$ (prediction) to $1.1 \cdot 10^{-3}$ m $h^{-1/2}$ (evaluation), the evaluated BTC for Cs-137 matches the measured data well (Figure 7-1c).

For Rb-86, we obviously have overestimated the retention in the matrix. The calibrated value of κ is $1.5 \cdot 10^{-4}$ m $h^{-1/2}$ compared to $2.2 \cdot 10^{-4}$ m $h^{-1/2}$ as used in prediction.

7.1.2 Path II

In the following we discuss the results obtained for tracer transport in Path II.

In Figure 7-2, the evaluated BTCs for the two sorbing tracers in path II are compared with the predicted BTCs and the measured data. The predicted and measured BTCs for the conservative tracer HTO are also presented.

The predicted BTC for HTO is higher than the measured BTC from the initial portion to the peak part. This deviation is interpreted as a result of hydraulic dispersion. When $<\tau>$ is increased from 200 h in the prediction to 270 h in the evaluation, and σ_τ is increased from 122 h^2 to 158 h^2 while keeping the coefficient of variation to be about the same, the evaluated BTC for HTO matches the measured data much better than the predicted BTC (Figure 5-2). The peak in the evaluated curve is still slightly higher than that of the measured data.

For Na-22, the predicted BTC deviates in the same way from the measured data as the predicted curve for HTO does from its measured data, with the deviation being much higher than for the case of Na-22 compared with that for the case of HTO. This implies that the deviation for the curves in the Na-22 case is due not only to hydraulic dispersion as in the case of HTO, but also to an underestimate of the retention in the rock matrix. By increasing κ from $2.4 \cdot 10^{-6}$ m $h^{-1/2}$ in the prediction to $6.0 \cdot 10^{-6}$ m $h^{-1/2}$ in the evaluation, the evaluated curve matches the meaured data very well (Figure 7-2a). Similarly for Ba-133, by increasing κ from $2.7 \cdot 10^{-5}$ m $h^{-1/2}$ in the prediction to $4.7 \cdot 10^{-5}$ m $h^{-1/2}$ in the evaluation, the evaluated BTC fits the measured data well (Figure 7-2b).

As is in the case of Path I, an increase of the calibrated κ in the evaluation also implies an enhancement of the sorption coefficient K_d, given the porosity being kept constant.

Table 7-1 compares predicted K_d values (Chapter 4) with evaluated values (Chapter 5) and the values obtained from penetration estimation (Chapter 6). The difference varies from a factor of 3 to 12.

Table 7-2 compares predicted (Chapter 4) and calibrated κ values (Chapter 5), as well as the estimated values from the penetration analysis (Chapter 6). The κ values are relatively close to each other, within a factor of 2.

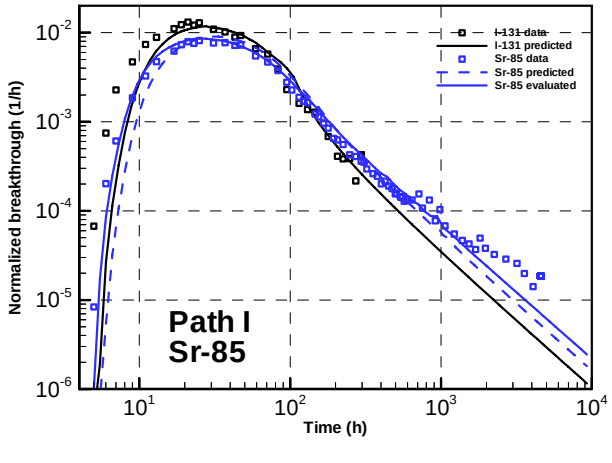

a

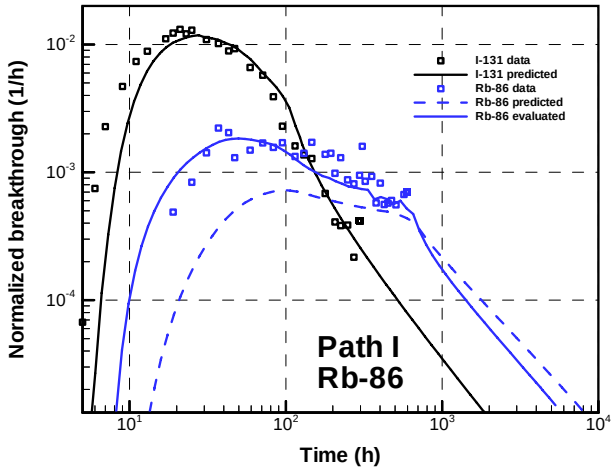

b

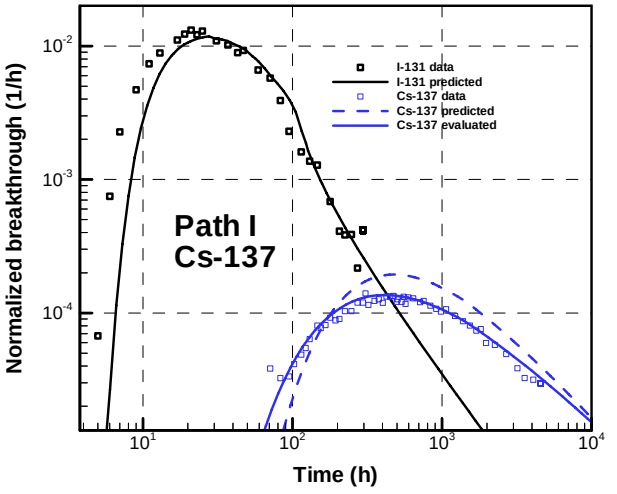

c

Figure 7-1. *The evaluated and predicted BTCs for tracers in Path I.*

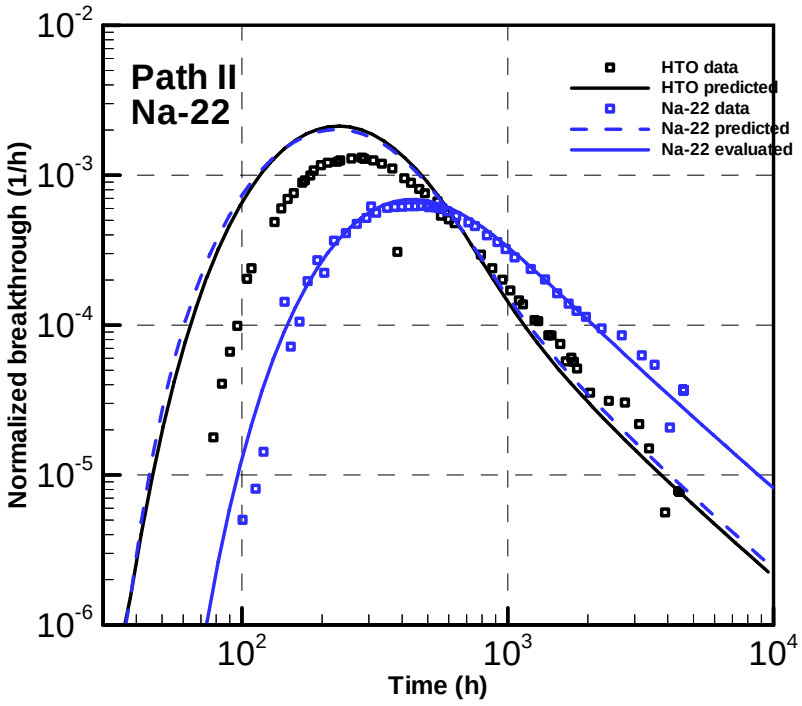

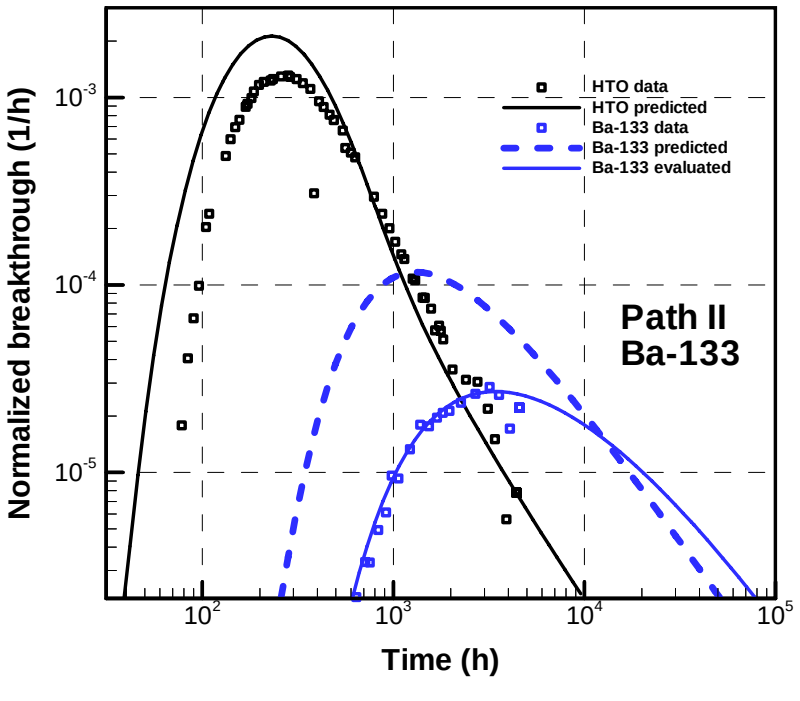

Figure 7-2. *The evaluated and predicted BTCs for tracers in Path II.*

Table 7-1. Comparison of K_d

Tracer	Sr-85	Na-22	Ba-133	Rb-86	Cs-137
	TRUE BS2B (Path I)	TRUE BS2B (Path II)	TRUE BS2B (Path II)	TRUE BS2B (Path I)	TRUE BS2B (Path I)
Predicted K_d (m^3/kg)	4.9e-5	1.7e-6	6.9e-4	1.1e-3	6.4e-3
Evaluated K_d (m^3/kg)	1.4e-4	2.1e-5	2.1e-3	5e-4	2.6e-2
Estimated K_d (m^3/kg)	1.5e-4	1.7e-6	6.9e-4	3.7e-3	1.2e-2

Table 7-2 Comparison of the κ parameters.

Tracer	Predicted κ [m $h^{-1/2}$]	Fitted κ [m $h^{-1/2}$]	Estimated κ [m $h^{-1/2}$]
Na-22	2.3e-6	6.0e-6	2.6e-6
Sr-85	3.1e-5	5e-5	6.8e-5
Ba-133	2.7e-5	4.7e-5	3.3e-5
Rb-86	2.2e-4	1.5e-4	4.8e-4
Cs-137	5.3e-4	1.1e-3	5.5e-4

7.2 Simple estimate of *k*

The calibrated mean and variance of water residence time for Path I are 12 h and 200 h^2, respectively. The coefficient of variation (CV) is thus 1.2. By assuming a linear β-τ relation in Path I, we obtain a slope k = 13000 $m^{-1}$from aperture estimate (Table 4-2).

The evaluated mean and variance of water residence time for Path II are 270 h and 25000 h^2 that give a CV of 0.6. The calibrated slope k for Path II is 17000 m^{-1} from estimation in Table 4-3.

In accordance with the definition of β, the slope k is equivalent to the inverse of an effective "retention" half-aperture. The evaluated k values yield an effective aperture 1/k of 0.15mm for Path I and 0.12 mm for Path II. For a rectangular streamtube, the value of τ can be estimated as V/Q where V is the volume of the streamtube and Q is the volumetric flow rate through the streamtube.

Let a streamtube have an effective half-aperture b_{eff}, a length L and a width W. Based on mass balance, we have the estimate:

$$\tau = \frac{2LWb_{eff}}{Q} \tag{7-1}$$

Consider first Path II. The evaluated travel time is 270 h, i.e., we set $\tau \approx 270$ h. The actual length of Path II is about 50 m as obtained from the DFN calculations (Fox et al., 2005) . Then W and b are related by

$$b = \frac{Q\tau}{2LW} = \frac{2.7Q}{W} \tag{7-2}$$

for a given Q. The flow rate in the injection section is 42 ml/h as given in Table 3-5 in Andersson et al (2004). Then W and b_{eff} can be computed using Equation (7-2). We choose the effective aperture ($2b_{eff}$) as an independent variable, and compute W values as summarized in Table 7-3.

The evaluated aperture of 0.12 mm (corresponding to our k=17000 1/m) gives a flow path width of about 2m if the flow rate is 42 ml/h. A flow path width of 2m is unreasonable, if the simple streamtube model is applicable. In the CPT-3 tests in the injection section KI0025F02:R2 (background fracture BG1), the natural flow is a constant of about 42ml/h (Andersson et al., 2004). This flow rate is surprisingly high considering the low transmissivity of the structure. Expected flow rates should be around 10 times lower (Andersson et al., 2004). In that case the flow rate for path II would be 4.2ml/h. The corresponding estimated aperture and width are given in the last two columns of Table 7-3 by assuming that the flow rate is one order of magnitude lower. The estimated width of the flow path would in this case be 0.2 m, which is deemed more reasonable for field conditions at hand. Thus the simple streamtube model in this case provides a reasonable estimate of k.

Table 7-3. Fracture aperture and width estimation for Path II.

***Q* = 42 ml/h**		***Q* = 4.2 ml/h**	
$2b_{eff}$ (mm)	W (m)	$2b_{eff}$ (mm)	W (m)
0.1	2.3	0.1	0.23
0.2	1.1	0.2	0.11
0.3	0.8	0.3	0.08
0.4	0.6	0.4	0.06
0.5	0.5	0.5	0.05

For flow path I, the path length is about 20m, the evaluated travel time is 12h.
The natural flow rate from tracer dilution for the injection section KI0025F02:R3 is 18ml/h (Andersson et al., 2004). A similar estimation using Equation (7-1) yields the corresponding values in Table 7-4. The evaluated aperture of 0.15mm gives a flow path width of 7.3 cm which is considered a realistic value.

Table 7-4 Fracture aperture and width estimation for Path I.

***Q* = 18 ml/h**	
$2b_{eff}$ (mm)	W (m)
0.1	0.11
0.15	0.073
0.2	0.055
0.3	0.037

7.3 Comparison of Structure #19 and background fracture BG1 flow paths

Flow path I is imbedded only in Structure #19, while flow path II starts from background fracture BG1 and ends in Structure #19.

Since the retention properties of Structure #19 (Flow path I) are much better characterized than those of background fracture BG1 (Flow path II), it is of interest to assess the possibility of inferring the retention properties of the background fractures and differentiate them from those of Structure #19.

Let flow path II, for simplicity, consist of two basic components: the part in BG1 and the part in Structure #19. The transport/retention through the entire system (flow path II) is then a convolution between transport in BG1 and transport in #19. Since we do not know the details of these flow path components, we shall omit the full convolution and rather use the simplified representation using the parameter group B [$h^{1/2}$], defined as $B = \beta\kappa = \tau k\kappa$.

It can be shown that for the convoluted transport, we have for flow path II, $B_{II} = B_{II}^{\#19} + B_{II}^{BG1}$ where B_{II} is the parameter B for the entire flow path II, while $B_{II}^{\#19}$ and B_{II}^{BG1} applicable for its subcomponents.

We have evaluated the κ and K_d values for tracers Sr-85, Rb-86 and Cs-137 in flow path I, and for tracers Na-22 and Ba-133 in flow path II. We would now like to infer κ and K_d values of tracers Sr-85, Rb-86 and Cs-137 for background fracture BG1. Likewise, we wish to infer κ and K_d values of tracers Na-22 and Ba-133 for Structure #19, in order to compare retention in the two structures. In Table 7-5 we show the calibrated (bold) and inferred values of κ for the tracers. It is assumed that K_d values for each flow path are proportional to the MIDS value (Byegård et al., 1998). In other words, it is assumed that the relative *ratios* between K_d values of the different tracers is preserved in the field and laboratory (MIDS). With this assumption, we can obtain K_d and κ values for all tracers in both flow paths as shown in Table 7-5.

In the following, we wish to estimate κ parameter for the background fracture BG1 by using $B_{II} = B_{II}^{\#19} + B_{II}^{BG1}$. By the definition of B for flow path II, we have the relationship:

$$\tau_{II} k_{II} \kappa_{II} = \tau_{II}^{\#19} k_{II}^{\#19} \kappa_{II}^{\#19} + \tau_{II}^{BG1} k_{II}^{BG1} \kappa_{II}^{BG1} \qquad (7\text{-}3)$$

We take Ba-133 as an example. From Table 7-5 and 5-3, we have $\tau_{II} = 270h$, $k_{II} = 17000m^{-1}$, and $\kappa_{II} = 4.7e\text{-}5\ mh^{-1/2}$. The left side of Equation (7-3) is thus known. If we assume that $\tau_{II}^{\#19} \approx \tau_I$, $k_{II}^{\#19} = k_I$ and $\kappa_{II}^{\#19} = \kappa_I$, i.e., the retention in Structure #19 of flow path II is approximately the same as the retention for path I. The first part in the right side of Equation (7-3) can also be constrained. From $\tau_{II} = \tau_{II}^{\#19} + \tau_{II}^{BG1} = 270h$, we have $\tau_{II}^{BG1} = 258h$. We need to know k_{II}^{BG1} in order to estimate κ_{II}^{BG1}. Since background fractures have generally smaller transmissivity it is reasonable to assume that $k_{II}^{BG1} \geq k_{II} = 17000m^{-1}$. In other words, the retention aperture in BG1 is at most the value for flow path II, or smaller, implying a larger k. With k_{II}^{BG1} =17000 1/m as the lower limit, an estimate of κ_{II}^{BG1} is 3.7e-5 $mh^{-1/2}$ which is in the order of our evaluation value of 4.7e-5 $mh^{-1/2}$, both being for Ba. By a similar estimation procedure, we can obtain κ values for BG1 for all tracers as shown in fourth column of Table 7-5. The parameter κ is systematically larger in Structure #19. The difference of κ between Structure #19 and BG1 is of a factor 2 to 9 given in last column in Table 7-5.

Table 7-5 Inferred κ [m $h^{-1/2}$] for Structure #19 and BG1 [for k (#19)=13000 and k(BG1)=17000 m^{-1}, respectively] .

Tracer	Structure #19 (path I) κ[m $h^{-1/2}$]	Path II κ[m $h^{-1/2}$]	Background fracture BG1	Ratio of κ
Na-22	3.9e-5	6e-6	4.9e-6	8
Sr-85	5e-5	8.4e-6	7.0e-6	7
Ba-133	3.3e-4	4.7e-5	3.7e-5	9
Rb-86	1.5e-4	1.0e-4	9.9e-5	2
Cs-137	1.1e-3	4.0e-4	3.8e-4	3

7.4 Hydrodynamic control of retention β

The parameter β quantifies the hydrodynamic control of retention processes for transport of tracers in fractures. For the purpose of this evaluation, we assumed a linear relationship of β and τ as $\beta = k\tau$. The slope k obtained from the evaluation is 13000 m^{-1} for Path I and 17000 m^{-1} for Path II (Table 5-3). Our estimation based on the flow rate earlier in this chapter indicates that these k values are reasonable. Using these k values and the estimated water residence times, we estimate the β values to be 1.6E+5 hm^{-1} for Path I and 4.6E+6 hm^{-1} for Path II. The estimate of β is more than one order of magnitude larger for Path II compared to the estimate of β for Path I. This is a natural consequence of smaller aperture and longer travel time of Path II. The parameter β depends only on the hydraulic condition. To compute β, we need aperture statistics and boundary conditions for flow. Thus these β values are only a rough estimation, and should be considered at best as an order of magnitude estimate.

7.5 Penetration analysis

Flow path I

There are several factors controlling the estimation of the κ value. The first one is the time *t* (Eq. 6-3). The second one is the definition of microstructure (e.g., thickness, porosity, and K_d in Table 6-11). A smaller κ value is due to either a longer time or a smaller θ, or even a smaller K_d. The time *t* was obtained from the evaluated BTCs in Chapter 5 and could not be known *a priori*. Should this method of analysis be used in prediction work, the time *t* has to be estimated from experiences or based on results of previous works. The definition of the immobile retention zones in Figures 6-2 and 6-3 is only conceptual. In reality the structure of the retention zones is more complex and irregular. All these factors are associated with large uncertainties. The analysis in this report should therefore be viewed as a preliminary attempt in addressing the heterogeneity normal to the fracture plane by making use of the microstructure model to obtain effective parameters.

The κ values estimated based on the penetration depth for all tracers are within 50% difference compared with the κ values evaluated through calibration in Chapter 5, except for Rb-86 where the difference is a factor of 3. Bearing in mind that there are so large uncertainties involved in this analysis, we consider the results to be consistent.

Flow path II

In the penetration analysis only the background fracture BG1 has been considered. The difference between the results of the two estimates in Table 6-18 is approximately within 50%. This indicates that the role of Structure #19 is limited. However, the underestimation of the κ value for the sorbing tracers is probably a result of having neglected Structure #19.

8 Conclusions

From the results of this work, the following conclusions can be drawn:

- The K_a values provided by Byegård and Tullborg (2004) give good predictions of the BTCs for all tracers in both flow paths except for tracer Na-22, where the K_a value has to be increased by a factor of 40 in the evaluation.
- The retention properties of the different rock materials as summarized by the parameter group kappa can be inferred reasonably well from the microstructural model and its parameterisation, i.e., independently of the tracer test results.
- The background fracture BG1 appears to have lower retention properties compared with Structure #19 as quantified by the effective parameter group κ. This suggests that the Type 2 structure may have weaker retention compared to the Type 1 structure. The difference for the parameter group κ is a factor of 2-9.
- The estimated retention half-aperture 1/k used in the prediction and evaluation for Flow path I is consistent with a simplified estimate based on a streamtube model with the effective width of the flow path of around 0.07 m (Eq. 7-1). For flow path II the flow rate appears uncertain; a consistent estimate of retention half-aperture 1/k is obtained with a streamtube model flow rate is on the order 2-4 ml/h.
- The estimate of β value of Path II is approximately one order of magnitude larger than the estimate of β for Path I.The tracers Na, Sr and Ba have K_d values (inferred) close to those obtained in the previous TRUE tests within a factor about 2. Tracers Rb and Cs have lower K_d values (inferred) compared to those obtained in the previous TRUE tests, the difference being about a factor in the range 5-10.

The conclusions associated with the hypotheses can be drawn as follows:

– **Hypothesis I a)** Microstructural (i.e. detailed geological, mineralogical and geochemical) information can provide significant support for predicting transport of sorbing solutes at experimental time scales.

  Our predictions were based on the calibration on the pre-test results for conservative tracers, and the microstructural model was not explicitly used. However, when using K_d and K_a values for the fracture rim zone of Structure #19, suggested by Byegård and Tullborg (2004), as effective values, good predictions could be obtained for the measured BTCs for sorbing tracers in Path I. When using the K_d and K_a values for the fracture rim zone of BG1, the modelling results underestimate the measured BTCs for all sorbing tracers. This suggests that the retention in Path II can be attributed to both Structure #19 and BG1.

– **Hypothesis I b)** Transport at experimental time scales is significantly different for faults (significant alteration, brecciation and fault gouge) and joints (with or without alteration), due to the indicated differences in microstructure and properties,

The evaluated porosity for Path I (2.6%) is much larger than the evaluated porosity for path II (0.43%). The penetration analysis gives the same results. The smaller porosity in Path II may be due to involvement of the background fracture BG1. This reveals the difference between faults (Structure #19) and joints (BG1). The longer evaluated travel time in Path II (270h) than in Path I (12h) could also be due to the difference in properties between the faults and joints.

In Path II, the penetration analysis by considering the background fracture BG1 only (negelecting Structure #19) underestimates the κ by 30% to 57% for sorbing tracers. This may indicate that the retention capacity in Path II comes from both Structure #19 and BG1. The higher porosity for Path I compared to Path I also suggests stronger retention for faults than for joints.

– **Hypothesis I c)** Longer distance pathways are dominated by fault rock zone behaviour, while shorter pathways (say representative for fractures in the vicinity of a deposition hole) may be more likely to be dominated by joint fracture characteristics.

As the Eulerian length of the two flow paths are approximately the same, we do not know the lengths of the actual trajectories in them. No conclusion can be drawn for this hypothesis.

– **Hypothesis II c)** Fracture retention properties tend to be scale-dependent primarily due to differences in microstructure.

For similar reasons as in Hypothesis Ic, no definite conclusions can be drawn for this hypothesis.

9 References

Andersson J., Elert M., Hermansson J., Moreno L., Gylling B., and Selroos J.-O. (1998). Derivation and treatment of the flow wetted surface and other geosphere parameters in the transport models FARF31 and COMP23 for use in safety assessment. Technical report R-98-60, SKB.

Andersson P., Gröhn S., Nordqvist R., Wass, E., (2004). TRUE Block Scale Continuation, BS2 Pretests. Crosshole interference, dilution and tracer tests, CPT-1 - CPT- 4. SKB International Progress Report IPR-04-25.

Andersson P., Byegård J., Nordqvist R., Wass E. (2005). TRUE Block Scale Continuation BS2B TRACER TESTS WITH SORBING TRACERS SKB International Progress Report IPR-05-01.

Byegård, J. (in prep). Sorption and leaching experiments using fault gouge and rim zone material from the Äspö Hard Rock Laboratory. Swedish Nuclear Fuel and Waste Management Company (SKB). Äspö Hard Rock Laboratory. International Progress Report IPR-0X-XX.

Byegård J., and Tullborg E.-L. (2004). Proposed sorption, porosity and diffusivity data for the modelling of the TRUE Block Scale Continuation sorbing tracer experiment. SKB. Unpublished internal Project data delivery #4.

Byegård J., Johansson H., Skålberg M., and Tullborg E.-L. (1998). The interaction of sorbing and non-sorbing tracers with different Äspö rock types: sorption and diffusion experiments in the laboratory scale. Technical report TR-98-18, SKB.

Bäckblom G., and Olsson O. (1994). Program for tracer retention understanding experiments, SKB HRL Progress Report, PR 25-94-24.

Cheng H. and Cvetkovic V. (2004). Modelling of sorbing tracer breakthrough for Tasks 6A, 6B and 6B2. Swedish Nuclear Fuel and Waste Management Company (SKB). Äspö Hard Rock Laboratory. International Progress Report IPR-04-30.

Cvetkovic V. (2003). Significance of diffusion limitations and rim zone heterogeneity for tracer transport through fractures at the Äspö site. TRUE Block Scale continuation project. International Progress Report IPR-03-43. Swedish Nuclear Fuel and Waste Management Company (SKB).

Cvetkovic V. and Cheng H. (2002). Evaluation of block scale tracer retention understanding experiments at Äspö HRL. Swedish Nuclear Fuel and Waste Management Company (SKB). Äspö Hard Rock Laboratory. International Progress Report IPR-02-33.

Cvetkovic V., Cheng H., and Selroos J.-O. (2000). Evaluation of Tracer Retention Understanding Experiments (first stage) at Äspö, International Cooperation Report, ICR-00-01, SKB.

Cvetkovic V., Selroos J.-O., and Cheng H. (1999). Transport of reactive tracers in rock fractures, J. Fluid Mech., 378, 335-356.

Dershowitz B., Winberg A., Hermansson J., Byegård J., Tullborg E.-L., Andersson P., and Mazurek M. (2003). Task 6C. A Semi-synthetic model of block scale conductive structures at the Äspö HRL. Swedish Nuclear Fuel and Waste Management Company (SKB). International Progress Report SKB IPR-03-13.

Fox, A, Dershowitz, W, Ziegler, M., Uchida, M. and S. Takeuchi 2006. BS2B Experiment – Discrete fracture and channel network modelling of solute transport modelling in fault and non-fault structures. Swedish Nuclear Fuel and Waste Management Company (SKB). International Progress Report SKB IPR-05-38.

Poteri A., Billaux D., Dershowitz W., Gómez-Hernández J-J., Cvetkovic V., Hautojärvi A., Holton D., Medina A. and Winberg A. (2002). Final Report of the TRUE Block Scale Project, 3. Modelling of flow and transport. Swedish Nuclear Fuel and Waste Management Company. Technical Report TR-02-15.

Selroos J. O., and Cvetkovic V. (1996). On the characterization of retention mechanisms in rock fractures, SKB Technical Report TR 96-20.

Tullborg E.L., Hermanson J. (2004). Assignment of distribution of geological structure type, complexity and parameters of the micro-structural model applicable to the predictive modelling of the BS2B sorbing experiment**.** Unpublished TRUE Block Scale Continuation Internal Technical Memorandum.

Winberg A., Andersson P., Hermanson J., Byegård J., Cvetkovic V., and Birgersson L. (2000). Äspö Hard Rock Laboratory, Final report of the first stage of the tracer retention understanding experiments. Technical report TR-00-07, SKB.